Neural Computations Leading to Space-specific Auditory Responses in the Barn Owl

Thesis by

Benjamin Jacob Arthur

In Partial Fulfillment of the Requirements

for the Degree of

Doctor of Philosophy

California Institute of Technology

Pasadena, California

2002

(Submitted October 1, 2001)

Acknowledgements

Thanks are due to Masakazu Konishi for guidance and support, to Roian Egnor, José Luis Peña, Mike Lewicki, and the rest of the Konishi lab for many useful discussions, to Kip Keller, Klaus Hartung, and Terry Takahashi for the generous use of their data, to Chris Malek for computer system administration, to Gene Akutagawa for histology, to Mike Walsh for electronics, to Herb Adams for machining, to Janet Baer, Robert Vega, and Luis Vega for animal care, to the National Science Foundation and the National Institutes of Health for funding, and to Masakazu Konishi, José Luis Peña, Sharad Shanbhag, and the Institute proofreader for comments on the manuscript.

Abstract

Sound localization is the ability to pinpoint the direction a sound is coming from based on auditory cues alone. Neurons in the brain which mediate this behavior are active only when sound comes from a particular direction. This thesis uses physiological and anatomical methods to investigate the computations which lead to such space-specific neural responses in the barn owl.

Chapter 3 studies a behavioral and neural phenomenon called phase ambiguity, which arises from the way in which the auditory nerve and cochlear nuclei encode acoustic information. Phase ambiguity causes errors in sound localization to be made for tonal stimuli, and is resolved through the convergence of information across different frequencies in broadband noise stimuli. Data presented here show that a continuous band of noise is not necessary; a set of tones spaced at the critical bandwidth resolves phase ambiguity just as well as a noise stimulus. This is due to a sub-linear interaction for tones of nearby frequencies.

Chapter 4 addresses the head-related transfer function (HRTF) model of sound localization. While traditional barn owl models use linear equations to relate interaural time differences (ITD) to azimuth and interaural intensity differences (IID) to elevation, the HRTF model purports that IID is dependent on frequency to such an extent that pattern recognition is used to match the spectral shape of IID in the stimulus to that characteristic of particular directions in space. Data presented here confirm predictions made by the HRTF model that IID tuning changes with frequency in space-mapped neurons, and that two-tone stimuli whose IIDs match these changes elicit better responses than those which do not.

Chapter 5 investigates the computation of space-specificity in the forebrain. Previous anatomical studies have suggested that the space-specificity seen there is not merely inherited from the space map in the midbrain, but rather arises, at least in

part, independently. The data presented here reconfirm that the forebrain pathway branches off from the midbrain pathway before the convergence across frequencies leads to space-specific neurons. All previous computations, however, including the formation of ITD-IID combination sensitivity, seem to be shared.

Collectively, these three studies expand our knowledge of the neurophysiology of sound localization in the barn owl by detailing specific mechanisms underlying the computation of space-specific neural responses.

Contents

List of Figures

List of Tables

Chapter 1 Introduction

Sound localization is a worthwhile and interesting field to study for not only is it an ability important to an individual's survival, but it is also a very well-defined computational task. There are two inputs, the sound pressure waveforms impinging on the ears, and one output, a physical movement, usually a saccade by either the head, arm, or eyes, indicating the direction of the sound's source. The computational means by which the sound direction is derived from the pressure waveforms has been studied for over two centuries using behavioral and physiological methods (Venturi 1796; Rayleigh 1876; Rayleigh 1906; Rosenzweig 1961). While most behavioral work has been done in humans, most physiological work has been done in other animals.

There are a variety of potential cues available in the two pressure waveforms which provide clues to the location of the sound source (Blauert 1997). These include both binaural cues, which are derived from differences between the two ears, and monaural cues, which rely on information conveyed by just one ear. Figure 1.1 shows a cartoon of how binaural cues arise. Interaural time differences (ITD) result from a longer pathlength to the far ear when a sound source is not on the midline. For frequencies whose wavelength is shorter than the head's diameter, interaural intensity differences (IID) may also arise due to diffraction. Monaural cues are due to reflections, and the resulting interference, within the outer ear that result in changes in the power spectrum of the stimulus.

In humans, psychophysical experiments have shown that while binaural cues mediate sound localization in the horizontal plane, monaural cues are used in the vertical plane (Middlebrooks and Green 1991). Both ITD and IID change with azimuth in the horizontal plane. However, due to the symmetry of the head about the midline, neither ITD nor IID change with elevation in the vertical plane, leaving only monaural spectral cues for the determination of a sound's elevation. Interestingly,

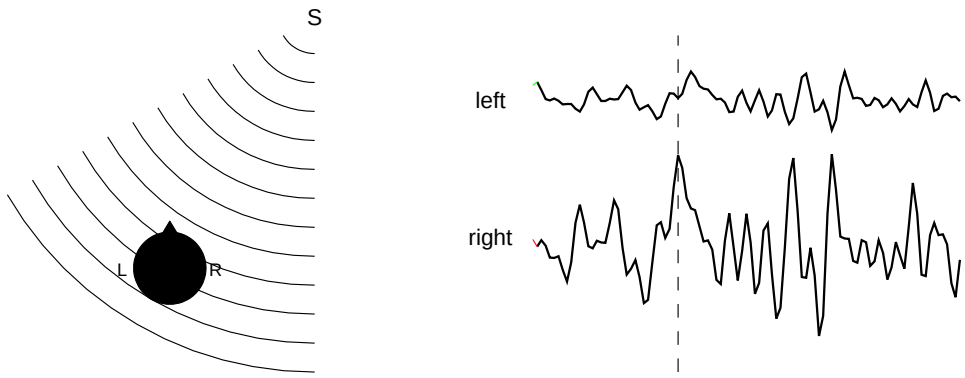

Figure 1.1: The ears can collectively be thought of as an interferometer. (left) A dorsal view of a listener with a sound source at a distance. (right) The sound pressure waveforms at the listener's ears. Note that the left waveform is smaller in amplitude and shifted forward in time relative to the right waveform.

the binaural cue used in the horizontal plane is frequency dependent: ITD is used for low frequencies and IID is used for high frequencies. This frequency dependence is called the duplex theory of sound localization, and is caused by phase differences being too small to discriminate at high frequencies and intensity differences being too small at low frequencies.

Sound localization has also been extensively studied in the barn owl (Knudsen 1981; Konishi 1993). While there are some similarities in the cues available to owls and humans for sound localization, the differences are quite striking, and are due to the asymmetry in the owl's ears (Norberg 1977). Ears can be thought of as directional microphones, and whereas in humans the peak sensitivity is symmetric about the midline, in barn owls, the left ear is more sensitive to sounds below the horizon while the right ear is more sensitive to sounds above the horizon (Payne 1971; Keller *et al.* 1998). This asymmetry has the effect of making IID encode elevation in the vertical plane. As a consequence, only ITD remains to encode azimuth in the horizontal plane. Moreover, monaural cues are not used by the owl for elevation (Egnor 2000).

The advantage of studying sound localization in owls is that behavioral studies can be combined with physiological experiments. Such experiments have demonstrated a map of auditory space in the midbrain (Knudsen and Konishi 1978a). This is a

profound discovery, for unlike visual maps of space in the forebrain, which are the result of topographical projections conserving the optically-produced retinal image, maps of auditory space must be computed from the tonotopic representation of sound pressure in the cochlea (Konishi 1986). Such auditory maps of space have since been found in several mammalian species, including guinea pig (Palmer and King 1982), cat (Middlebrooks and Knudsen 1984), bat (Wong 1984), and ferret (King and Hutchings 1987).

Experiments designed to elucidate the nature of the computations leading to the auditory space map have demonstrated that ITD and IID are processed in parallel pathways in the barn owl (Moiseff and Konishi 1983; Takahashi *et al*. 1984). These computational pathways are separated at the cochlear nuclei, both of which receive bifurcating axonal projections from the auditory nerve (Carr and Boudreau 1991). Neurons in these two cochlear nuclei, nucleus magnocellularis (NM) and nucleus angularis (NA; Fig. 1.2), are narrowly tuned to frequency and collectively encode an approximation to a Fourier transform: NM neurons preserve timing information by locking their spikes to the phase of the stimulus (Sullivan and Konishi 1984; Köppl 1997), while NA neurons encode the magnitude of the stimulus with the large dynamic range of their spike rate (Sullivan and Konishi 1984). NM and NA project to nucleus laminaris (NL) and nucleus ventralis lemnisci laterale, pars posterior (VLVp), respectively (Takahashi and Konishi 1988a; Takahashi and Konishi 1988b). These nuclei, though still narrowly tuned to frequency, are the first nuclei in the auditory pathway that receive binaural inputs. NL neurons encode interaural phase differences with their spike rate using coincidence detection on the bilateral axonal delay lines from NM (Moiseff and Konishi 1983; Carr and Konishi 1988). VLVp neurons use a positive feedback loop consisting of mutual bilateral inhibition to encode IID with a sigmoidal function of their spike rate (Moiseff and Konishi 1983; Manley *et al*. 1988; Takahashi and Keller 1992). NL and VLVp both project to the central nucleus of the inferior colliculus (ICc) in the midbrain (Takahashi and Konishi 1988b; Takahashi and Keller 1992; Adolphs 1993b), where neurons narrowly tuned to frequency are arranged tono-

topically (Knudsen and Konishi 1978b). While the terminals from NL are confined to a subdivision of ICc called the core, those from VLVp are confined to the medial and lateral shell subdivisions. Since core projects to lateral shell (Takahashi *et al.* 1989), neurons there are sensitive to both time and intensity differences (Feldman and Knudsen 1994; Mazer 1995; Keller and Takahashi 2000). The interaction between these binaural cues is multiplicative and can be thought of as an AND gate: neurons only spike when both time and intensity differences are favorable (Peña and Konishi 2001). While only the lateral shell subdivision of ICc projects to the external nucleus of the inferior colliculus (ICx), all three subdivisions project to nucleus ovoidalis (NO), part of the thalamus (Knudsen and Knudsen 1983; Proctor and Konishi 1997; Cohen *et al.* 1998). This split in the flow of information gives rise to the midbrain and forebrain pathways, respectively, both of which contain space-specific neurons that are broadly tuned to frequency (Fig. 1.2). In the midbrain pathway, these space-specific neurons are found in ICx and the optic tectum (OT; Knudsen and Konishi 1978a; Knudsen 1982). In the forebrain pathway, space-specific neurons are found in the auditory region of the archistriatum (AAr; Cohen and Knudsen 1995), to which NO projects indirectly via field L (Cohen *et al.* 1998). What differs between these two pathways is that while ICx neurons are not only space specific, but also arranged into a map of auditory space, AAr neurons, though space specific, have a "patchy" map of space. The auditory space map in ICx arises developmentally through an alignment with the visual space map in OT (Knudsen 1983a; Knudsen and Knudsen 1985; Knudsen and Brainard 1991). Space specificity, at least in ICx, is due in part to a convergence across frequency channels, which creates neurons broadly tuned to frequency and turns a sensitivity to interaural phase difference into a sensitivity to ITD (Takahashi and Konishi 1986).

This thesis consists of three projects: two physiological experiments studying spectral convergence in ICx and its relation to ITD and IID processing, and an anatomical study of the projection of IC to NO. (1) Previous studies in ICx have demonstrated the importance of the stimulus bandwidth for creating unambiguous neural responses

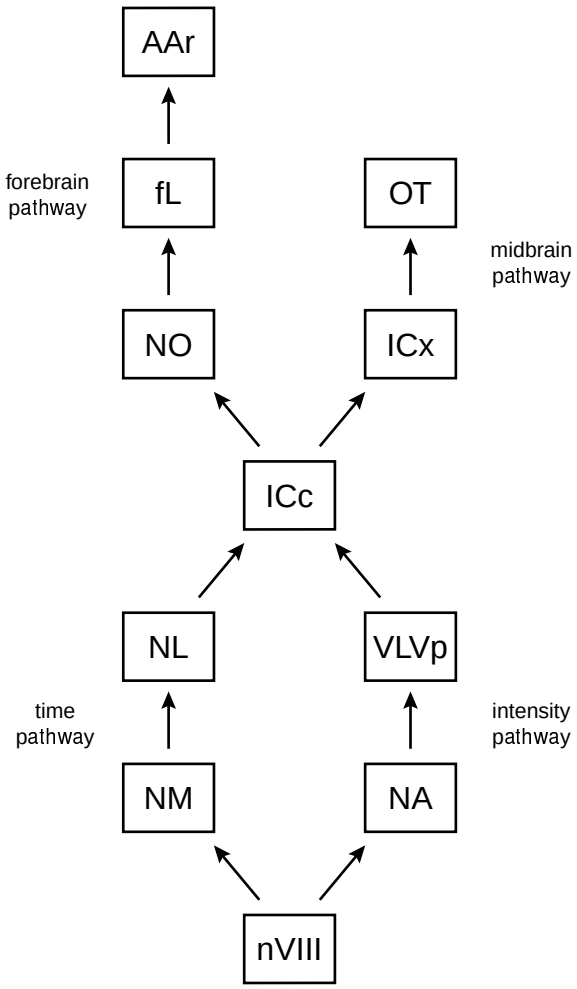

Figure 1.2: A schematic diagram of the pathways mediating sound localization. Auditory nerve afferents (nVIII) bifurcate and send collaterals to both the time and intensity pathways. Interaural time (ITD) and intensity (IID) difference cues are processed separately in these pathways until they converge on the nucleus of the inferior colliculus (ICc). Though some ICc neurons are sensitive to both ITD and IID, none are space-specific. ICc projects, however, to both the midbrain and forebrain pathways, each of which contains space-specific neurons. Nucleus magnocellularis (NM); nucleus angularis (NA); nucleus laminaris (NL); nucleus ventralis lemnisci lateralis, pars posterior (VLVp); external nucleus of the inferior colliculus (ICx); optic tectum (OT); nucleus ovoidalis (NO); field L (fL); auditory archistriatum (AAr).

to ITD (Takahashi and Konishi 1986). Chapter 3 describes experiments using two- and multi-tone stimuli designed to elucidate how the interaction between tones within a noise stimulus resolves phase ambiguity. (2) The diffraction of sound around the head is frequency dependent and causes IID cues to vary with frequency (Keller *et al.* 1998). While recent studies have demonstrated that IID tuning in ICx changes with frequency (Gold and Knudsen 2000; Euston and Takahashi 2002), Chapter 4 describes experiments which again use two-tone stimuli to investigate whether these changes in IID tuning have any significant ramifications. (3) It is currently believed that the central, but not the external, nucleus of IC projects to NO (Knudsen and Knudsen 1983; Proctor and Konishi 1997; Cohen *et al.* 1998). This implies that the space-specific properties of neurons in AAr arise *de novo*, independent of those in ICx and OT. Chapter 5 addresses this issue by using fluorescent retrograde tracers to study in detail the distribution of OT and NO efferents within IC.

Chapter 2 Methods

Single-neuron extracellular recordings were made in repeated acute experiments in nine anaesthetized adult barn owls (*Tyto alba*). Retrograde labelling studies were performed in five of these owls on the side contralateral to the physiological recordings.

Surgery

Prior to data collection, owls were prepared for recording sessions by installing a head plate and a zero post. Owls at least six months old were selected from a breeding colony and starved overnight. The next day the owls were anaesthetized with intramuscular injections (27G-1/2; 1 mL; Becton Dickinson) of ketamine (10 mg; Ketaject; Phoenix Pharmaceuticals) and diazepam (0.5 mg; Abbott Laboratories) and given a preventative dose of oxytetracycline (20 mg; maxim-200; Phoenix Pharmaceuticals) intramuscularly. Supplemental injections of ketamine (10 mg) and diazepam (0.25 mg) were administered as needed. Respiratory rate and movement were used as indicators of the depth of anaesthesia. A water-based heating pad (k-20-f; American Medical Systems) was used to maintain body temperature. The wings were restrained with a soft leather jacket and knee flexion was prevented using plastic tubes (3 cm diameter, 15 cm long, cut graduated cylinder). The feathers on the dorsal surface of the cranium were plucked. The facial ruff feathers were left intact. Ear bars and a beak holder were used to firmly hold the head in place with the beak rotated in the sagittal plane 30 degrees ventrally from the horizontal plane. The scalp was cleaned with chlorhexidine (0.05%; Fort Dodge Laboratories) and an incision was made along the midline. Surgical tools (Roboz, Fine Science Tools) were sterilized with an autoclave (57CR; American Sterilizer) before the start of each procedure and aseptic conditions were maintained through the liberal use of a hot bead sterilizer (250; Si-

mon Keller). The top layer of the skull was removed with rongeurs. A stainless-steel inverted-T-shaped headplate (custom; Central Engineering Services, CES, Caltech) was affixed to the underlying trabeculae with dental cement (perm reline and repair resin; Hygenic Corp.). Posterior to the headplate a stainless-steel 0.25-mm-diameter zero-post wire was similarly attached to the skull on the midline and in the coronal plane containing the interaural axis. Anterior to the headplate a stainless-steel hypodermic tube (1.1 mm OD, 0.7 mm ID; 19 gauge; Small Parts) was similarly attached to the skull to vent the middle ears and interaural canal through the trabeculae. 0.5% bupivacaine (sensorcaine MPF; Astra USA) was applied to the edges of the wound and silk thread (4-0 a-53; Ethicon) was used to suture it closed. Owls were placed in a heated recovery cage overnight. A polyvinyl-chloride tube (11 cm diameter; PVC) was used to restrain them until they were awake enough to crawl out of it.

Recording sessions typically lasted all day. Owls were starved overnight as before. Initial injections of anaesethetics were as before and supplemental injections consisted of only ketamine. The head plate was used to bolt the owl's head to a stereotaxic system (custom; CES). Tools were cleansed as before. The external nucleus of the inferior colliculus (ICx) was approached through one of two methods: the normal approach and the posterior approach. In the former, the head was kept tilted at 30 degrees, the sutured wound was reopened, and a small craniotomy was made 5 mm lateral to the zero post. The dura was resected with a hypodermic needle and an electrode lowered to a depth of about 12-14 mm from the surface of the brain. After the recordings were finished, the brain was covered with gelfoam (Pharmacia and Upjohn), the craniotomy was sealed with dental cement, sensorcaine was applied to the wound, and it was sutured shut. In the posterior approach the head was rotated an additional 70 degrees ventrally for a total of 100 degrees. A small incision was made along the posterior edge of the ruff over the middle ear cavity, which is just dorsal of the posterior end of the jawbone. The cavity was opened with rongeurs to expose the optic lobe. A small handheld drill bit was used to remove the bone over the tectum, the dura was resected with a hypodermic needle, and an electrode lowered to

a depth of about 2-3 mm. The back end of the electrode was angled 45 degrees laterally in the vertical plane perpendicular to the midline and 10 degrees posteriorly in the horizontal plane. After the recordings were finished, a small piece of polystyrene (weigh boats; VWR Scientific) was affixed with cyanoacrylate glue (superglue; Loctite Corp.) over the hole leading into the middle ear cavity, sensorcaine was applied to the wound, and it was sutured shut. For both approaches, owls were given an additional dose of oxytetracycline, buprenorphrine (0.015 mg; buprenex; Reckitt and Colman Pharmaceuticals) intramuscularly, and 10 cc of either 5% dextrose (Abbott Laboratories) in physiological saline (Baxter Healthcare) or lactated ringer's solution (B. Braun Medical) subcutaneously before being placed in the recovery cage.

These procedures comply with guidelines set forth by the National Institutes of Health and the Institute Animal Care and Use Committee of Caltech.

Electrodes

Carbon fiber electrodes were made using protocols first described by Armstrong-James and Millar (1979). Briefly, a silver-plated solid-copper wire (30 gauge, 0.3 mm diameter; wire-wrap wire; Digi-Key) was threaded through a borosilicate glass pipette with no filament (1 mm OD, 0.58 mm ID; 1B100-4; World Precision Instruments). A single strand of high-modulus carbon fiber (5 μm; pyrofil HS40; Grafil) was silver printed (22-201; GC Electronics) to the protruding wire. The carbon fiber was pulled back into the glass pipette which was then heated and pulled (720; David Kopf Instruments) until it collapsed around the carbon fiber and broke. The protruding carbon fiber was coarsely trimmed with a scalpel and, with a microscope, was pulled back into the pipette such that the glass extended beyond the fiber while the fiber still remained firmly grasped by the collapsed portion of the pipette. The tip of the carbon fiber was re-exposed by bumping the glass tip up against a glass slide underneath a microscope until 10-15 μm protruded. This procedure minimized the shunt capacitance through the shank of the electrode by reducing the length of the thin glass insulation in direct contact with the carbon fiber. The tip was then

made watertight by passing it through an alcohol flame for less than 1 second. The back end of the electrode was sealed with cyanoacrylate glue. Electrodes were heated at 300 C (HL-1800E; Steinel) for 3 hours to remove epoxy applied during the manufacture of the carbon fiber, activated using +0.5 nA DC (custom) in 1% KNO_3 (Mallinckrodt Chemical) for 3 hours (Pittman *et al.* 1999), and then plated with platinum using -100 nA DC (custom) in 0.2% $PtCl_6$ (Sigma) for 45 seconds in a sonicator (B-12; Branson; Marrese 1987). Resulting impedances were less than 1 MΩ and neurons with 1 mV peak-to-peak spikes and 50 μV peak-to-peak background noise were routinely isolated for an hour. With practice, an electrode could be manufactured in 15 minutes and the yield was about 1 in 2-3. Used electrode tips were reconditioned by shocking with +9 V DC (Duracell) for less than a second and/or sonicating in 1% HCl (Mallinckrodt Chemical) for about a minute. In preliminary experiments, various other electrode designs were tried, including tungsten (Hubel 1957), electrolyte-filled glass (NaCl, KCl, NaAcetate, KAcetate, from 0.15 to 5 M), and Wood's metal (Dowben and Rose 1953). None performed as well as, or had all of the desirable characteristics (minimal shank capacitance, low tip impedance, physiologically inert, high durability) obtainable with, carbon fiber.

Rig

The sound delivery system consisted of a computer (sparc IPX; Sun Microsystems), a stereo digital-to-analog converter (DAC; proport 656; Ariel), a pair of programmable digital attenuators (PA4; Tucker Davis Technologies, TDT), a stereo amplifier (HB6; TDT), a stereo high-pass attenuator (custom), and a pair of miniature speakers (ED-1914 and BF-1743; Knowles) encased in an aluminum housing (custom; CES) and sealed in the ears with silicone (gold velvet II; All American Mold Laboratories). A small venting gap was left in the sealant so that pressure would not build up inside the ear canal. The DAC sampled the waveform at 48 kHz with a 16-bit resolution. The programmable attenuators were adjusted by the computer on a trial-by-trial basis to set the average binaural intensity (ABI) and interaural intensity difference (IID).

The high-pass attenuator was needed to bring the overall output level of the speakers down to the lower part of the owl's hearing range. It consisted of a passive first-order high-pass filter with a cutoff frequency well above 12 kHz to compensate for a peak in the output of the speakers at 3 kHz.

The front end of the neural recording system consisted of a headstage (μA-108; BES) and a filter (PC1; TDT). The output of the filter was split three ways and sent to an oscilloscope (5115; Tektronix), an audio monitor (AM8; Grass), and the computer via an analog-to-digital converter (ADC; proport 656; Ariel). The headstage was a 10x-voltage-gain current buffer with a 0.5 Hz high-pass filter. The filter was a 1-10 kHz second-order bandpass filter and had an additional 100x voltage gain. The ADC used the same clock as the DAC and so the two were synchronized.

All recordings were performed in a double-walled soundproof chamber (outside 1.2 x 1.6 x 1.4 m, inside 0.5 x 0.8 x 0.6 m; Acoustic Systems). Inside the chamber was a stereotaxic system (custom; CES), a micromanipulator (461; Newport), and a microdrive (μD-100; BES and CES). The medio-lateral and antero-posterior position of the electrodes was set with the micromanipulator using stereotaxic coordinates. The dorso-ventral position was done under physiological guidance with the remote-controlled microdrive.

Custom software was used to discriminate spikes in real time. Single neurons were identified on the basis of a refractory period (Fig. 2.1) and a similar spike shape. They were discriminated from other spikes and noise using a software level detector and, if necessary, up to three optional dots which specified a spike shape. Each spike was assigned a timestamp which was stored in a computer file. An inter-spike interval histogram and a graph of overlayed spike waveforms aligned at the peaks were updated with each stimulus presentation. This allowed isolation quality to be monitored in real time. Plots of tuning curves were generated immediately after the data were collected and the computer files could be used for more extensive analysis later.

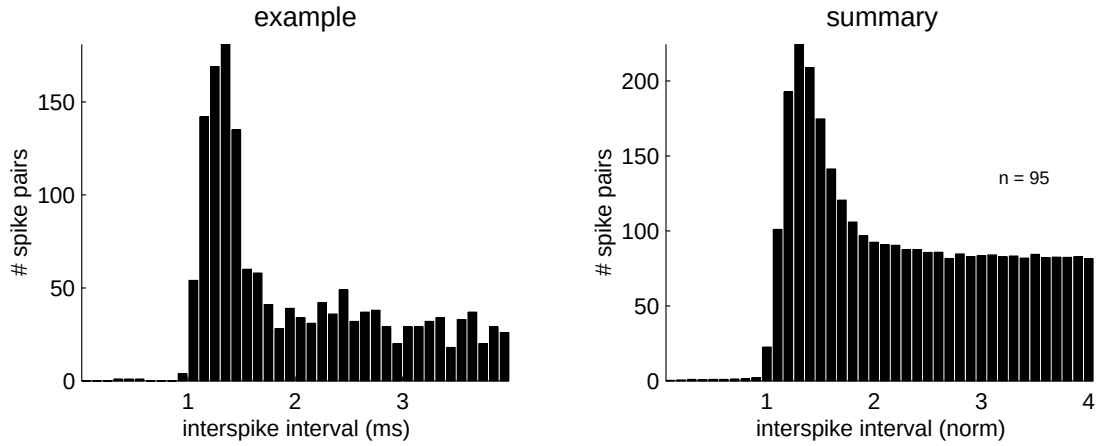

Figure 2.1: Interspike interval histograms. (left) A specific example (owl 689, neuron 15) for which there were three spike pairs (0.0524% of the total) in the refractory period during a 61-minute recording. (right) A summary of 95 neurons, formed by scaling the x-axis by the refractory period and then taking the mean. Overall, the spike pairs occurring within the refractory period accounted for only 0.222% of the total. Average isolation length was 72 ± 43 (std. dev.) minutes.

Stimuli

Custom software was used for the synthesis of stimuli. It was written in C in a unix environment (SunOS 4.1, Red Hat Linux 5.2) and is freely available via anonymous ftp from etho.caltech.edu (/pub/xdphys). Stimuli consisted of 100 ms sounds with 5 ms linear rise and fall ramps. Spikes were recorded 100 ms before the stimulus onset and 200 ms after stimulus offset. Stimuli were presented once per second. Noise was synthesized by specifying the desired amplitude and phase spectrum and then doing an inverse Fourier transform. One- and two-tone stimuli were synthesized in the time domain. Phases were randomized between trials and, in atonal stimuli, across frequencies. For noise stimuli a 200 ms sound was synthesized in advance and cached. Each repetition of these stimuli pulled a different 100 ms section out of the cache. The intensity of noise and pure-tone stimuli was adjusted such that the overall RMS amplitude (a.k.a. average binaural intensity, ABI) was identical for a specified intensity. This resulted in the power spectral density of noise stimuli being much smaller than that of pure-tone stimuli. Each of the tones in two-tone and multi-

tone stimuli, on the other hand, had an intensity identical to that of the one tone in pure-tone stimuli for a specified intensity (except for Figure 3.9, right column). This resulted in two-tone stimuli being 3 dB louder than pure-tone stimuli, and allowed their responses to be directly compared to pure-tone responses.

With the exceptions noted in the next paragraph, stimuli were grouped into sets in which only one parameter was varied. These stimulus sets are called tuning curves, for they quantify to which values of the parameter the neuron responds. ITD tuning curves, for example, consisted of a set of stimuli in which ITD was varied over the behaviorally relevant range, while keeping IID, ABI, and the spectrum constant. Each ITD was presented ten times and all the stimuli were randomized such that each ITD was presented once before any were played again. Similar procedures were used to take IID, ABI, and frequency tuning curves. ITDs were sampled every 30 μs, IIDs every 3-6 dB, ABI every 5 dB, and frequency every 125-500 Hz. IID and frequency were both sampled with finer resolution near the value which elicited the maximum response, and coarser resolution elsewhere. Positive ITDs and IIDs represent sounds which were leading and louder, respectively, in the right ear. The words "contra" and "ipsi" in x-axis labels indicate which ITDs lead, and which IIDs were louder, in the contralateral and ipsilateral ear, respectively, relative to the side of the brain in which the neuron was being recorded. It is important to remember that the neural responses illustrated in a tuning curve depend on the values of the fixed parameters. In this sense, tuning curves don't indicate all the values of a parameter to which a neuron is sensitive, but only those to which it is sensitive given the values chosen for all of the fixed parameters.

For certain protocols, the data were collected in an interleaved fashion. This was done to avoid the confound of neural tuning changing with time, which could happen, for example, due to changes in the depth of anaesthesia or in the health of the cell. The data of Figure 3.1 are from one such interleaved protocol. All of the curves were taken simultaneously, hence any differences between them cannot be attributed to changes in neural tuning with time. Other figures in which the data were interleaved

include Figures 3.2, 3.4, 3.8, 3.9, 4.6, 4.1, 4.2, 4.3, 4.7, and 4.9.

Calibration

Stimuli were calibrated to produce a specified intensity independent of the frequency response of the speakers. The frequency response of the speakers was measured *in situ* immediately before and after each neuron was isolated. The speaker calibration system consisted of miniature microphones (EA-1939; Knowles) and a stereo microphone amplifier (custom; BES). The microphones were encased in the same custom aluminum housing that the miniature speakers were in, each having a separate cavity within that housing and a separate acoustic pathway leading to the ear canal. The output of the microphone amplifier was manually switched into the ADC and replaced the neural signal during calibration. Tones were played individually from 0.5 to 12 kHz and a software-based phase-locked amplifier was used to ascertain the magnitude and phase of the tone (Fig. 2.2, left). Neurons for which the before and after calibration curves were different were thrown out (Fig. 2.2, right). Venting of both the ear canal and the middle ear was crucial to obtaining stable calibrations, an observation also made by Keller *et al.* (1998) and Carlile (1990). The inverse of the speaker output was used to digitally filter the outgoing stimuli to effectively make the speakers flat. For noise stimuli the spectrum was multiplied by the inverse of the speaker's response before doing the inverse FFT, while for tones the digital attenuators were used to compensate for the magnitude, and a constant was added to the argument of the sine function to compensate for the phase. The microphones with which the speakers were calibrated were not flat, but were calibrated against a flat microphone (4133, 2801; Brüel and Kjær) in free-field conditions. The inverse of this calibration data could be used to transform the microphone's output into what a flat microphone would have given, thus obviating the need to use a large and expensive flat microphone for speaker calibration on a daily basis.

Stimuli were not adjusted to negate the transfer function of the ear canal. Sound exited the aluminum housing just lateral to what Keller *et al.* (1998) called the outer

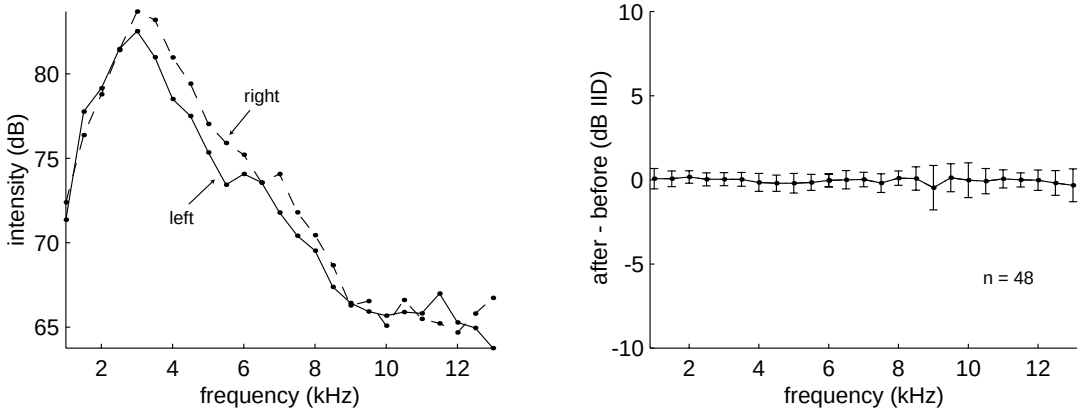

Figure 2.2: Calibration data for the dichotic speakers. (left) Variation in sound pressure level (re 20 μP) for the left (solid) and right (dashed) speakers, as measured *in situ* by calibrated microphones immediately adjacent to the speakers. The peak at 3.5 kHz is followed by a 10 dB per octave rolloff, whose magnitude has been lessened by a passive first-order high-pass filter with a cutoff frequency above 12 kHz. (right) The difference between the calibration data before and after a neuron was isolated showing that the frequency response of the speakers was time invariant to within 1 dB for the duration of the recording. Plotted is an average of 48 curves, formed by taking the difference of the two curves in the left panel to form the IID of the calibration data, taking the difference between the IID of the calibration data collected before and after each neural isolation, and then taking the mean. Error bars indicate the standard deviation.

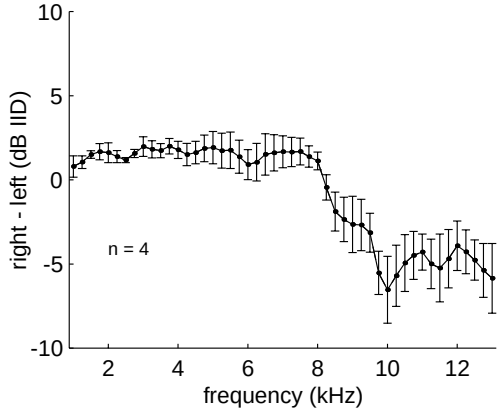

Figure 2.3: The frequency response of the ear canals, as measured with probe tube microphones near the tympanum and headphone microphones at the entrance of the canal near the speaker. Plotted is the average difference between the frequency responses of the right and left ear canals for four owls, indicating the artifactual IID resulting from calibrating the speakers at the entrance of the canal.

shelf. This is about 15 mm from the columella through an S-shaped canal. As the transfer function of this canal has not previously been reported, it was measured here through the use of probe tubes surgically implanted through the squamosal bone. Probe tubes were constructed from hypodermic stainless-steel tubing (1.1 mm OD, 0.7 mm ID; 19 gauge; Small Parts) and implanted such that one end was medial to the inner shelf of Keller *et al.* (1998) and about 1-2 mm from the tympanum, while the other end protruded through the squamosal bone and skin to the posterior surface of the head. Miniature speakers, attached to the probe tubes with a short length of polyethylene tubing (intramedic; Becton Dickinson), were then used to measure the transfer function of the ear canal with the speakers and aluminum housing placed lateral to the outer shelf just as they were during recording sessions. While the transfer functions for each ear showed some variability, the difference between the left and right ear canals were surprisingly similar despite uncontrollable variation in the exact placement of speakers and probe tubes. Figure 2.3 shows summary data for which the difference between the left and right ear canal's transfer function was averaged across four owls. There is a transition from +1 dB to -5 dB IID at 9 kHz. This adds some artifact to the data of Figure 4.3, but only for those neurons in which frequencies above 9 kHz were sampled. It had negligible effect on the summary data of Figure 4.4 and no effect on the conclusions.

Tracer Injections

Fluorescein- and tetramethylrhodamine-conjugated dextran amines (FDA and RDA, respectively; 3000 MW, anionic, lysine fixable; D-3306, D-3308; Molecular Probes; Gimlich and Braun 1985) were microiontophoretically injected into the optic tectum (OT) and nucleus ovoidalis (NO). Single-barrelled glass pipettes with 15-20 μm tip sizes were filled with a 10% solution of either FDA or RDA in 0.2 M KCl. An 85 V battery was used to apply +20 μA DC for 20 minutes. The current was pulsed on and off every 7 seconds using a custom device (BES). NO was found a week prior to the injections using 3 M NaCl glass electrodes with 7-10 μm tip sizes. The

normal approach was used and NO was usually found about 2 mm lateral and 2 mm anterior to the zero post, and about 12 mm below the surface of the brain. Injections were made under physiological guidance by recording through the injection pipette. OT injections were made later on the same day using the posterior approach. The electrode was positioned under visual guidance and the injections were made about 1200 μm below the surface of the brain. With one exception multiple injections were made into each nucleus of each owl. All injections into a given nucleus were of the same tracer (i.e., either FDA or RDA), and within an owl, NO and OT always received different tracers. Which nucleus received which tracer was alternated with each owl.

A confocal laser-scanning microscope (310; Zeiss) was used to examine the sections. The injection protocol not only resulted in the iontophoresis of tracer, but also created a lesion, easily visible under darkfield microscopy. Retrogradely-labelled cells were visualized with fluorescent laser-scanning microscopy in the IC that was contralateral to the side in which physiological recordings were made. The 488 nm line from an argon-ion laser in conjunction with a 500-550 nm bandpass emission filter (Chroma Technology) was used to scan for FDA. Similarly, the 543 nm line from a helium-neon laser in conjunction with a 560-620 nm bandpass emission filter was used to scan for RDA. Brightness and contrast settings for the photo-multiplier tubes were set using the injection sites as positive and negative controls. Even for the brightest settings, these combinations of tracers, lasers, and filters produced virtually no cross-talk. Only the brightest cells, those which saturated the photo-multiplier tubes, were counted as labelled. This is a conservative estimate of the total, as there were many cells that contained slight amounts of tracer that did not meet this strict criterion.

Histology

Recording sites were verified histologically (Fig. 2.4). At the end of the last session, a pair of electrolytic lesions in IC were made 1 mm apart in the same dorso-ventral electrode tract by passing -50 μA DC (custom) for 10 seconds twice. Three days later

the owls were overdosed with sodium pentobarbital (30 mg; nembutal; Abbott Laboratories) and perfused through the left ventricle with physiological saline followed by 2% paraformaldehyde (Fisher Scientific). The brain was removed, allowed to postfix overnight, and then sunk in 30% sucrose for two days. 60 μm sections were cut (860; American Optical) and mounted (permount; Fisher Scientific; or, for fluorescence, vectashield; Vector Labs). Darkfield microscopy (optiphot; Nikon) was used to verify that the lesions were in IC. Camera lucida drawings were made for all lesions, and digital photomicrographs (axiocam, axioskop; Zeiss) taken of selected lesions for use in figures.

Analysis

Analysis was done using custom software written in Matlab 5.3 (The Mathworks), and figures were made using Illustrator 9.0 (Adobe) and Photoshop 5.0 (Adobe).

The terms facilitation and suppression are defined as the extent to which the response to the two-tone stimulus exceeded or fell short of the response to the fixed tone played alone. The terms super- and sub-linear are defined as the extent to which the response to the two-tone stimulus exceeded or fell short of the sum of the responses to the two tones played individually. Note that while all super-linear responses are facilitative, and all suppressive responses are sub-linear, only some sub-linear responses are suppressive and only some facilitative responses are super-linear. However, when the response to one of the tones played alone is zero, facilitative is identical to super-linear, and suppressive is identical to sub-linear.

The terms facilitation and suppression are also used with regard to the noise versus best-frequency (BF) ITD tuning curves of Figure 3.1, despite being technically inaccurate in those circumstances. Facilitation and suppression both usually refer to the change in the response to a stimulus when that *exact same* stimulus is presented in the context of a second stimulus. In the case of facilitation and suppression at the main and side peaks, one is interested in the difference in the responses to the BF alone and to the BF plus all of the other frequencies in the noise. But in Figure 3.1, the

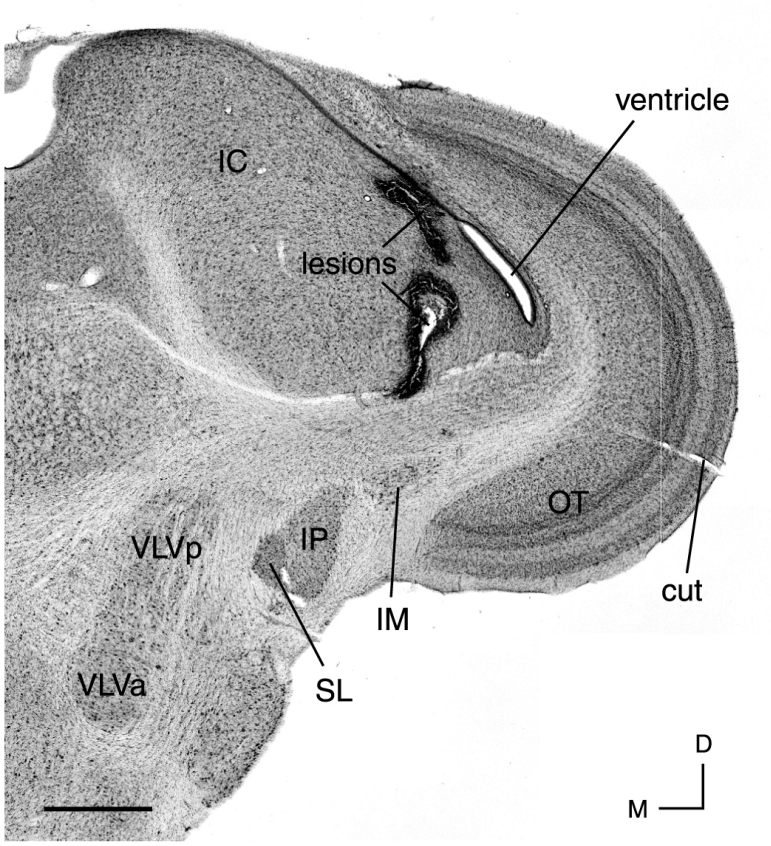

Figure 2.4: Electrolytic lesions verifying the recording sites. Shown is a montage of 11 brightfield photomicrographs of a 60 μm-thick cresyl-violet stained coronal section from owl 685. Note the pair of lesions in lateral IC, made 1 mm apart in the same dorsal-ventral penetration. Dorsal is up; medial is left; scale bar is 1 mm. Inferior colliculus (IC); optic tectum (OT); magnocellular and parvocellular subdivisions of the isthmal nucleus (IM and IP, respectively); nucleus semilunaris (SL); nuclei ventralis lemnisci laterale, pars anterior and posterior (VLVa and VLVp, respectively). The knife cut in the ventrolateral part of OT was used to identify left from right when mounting.

noise and pure tone stimuli were normalized such that the overall RMS intensity (i.e., ABI) was the same, independent of the bandwidth of the stimulus. This means that the intensity at the BF in the noise stimulus is much quieter than for the BF presented alone. The BF stimulus, then, is not *exactly* the same in both conditions, and so the terms facilitation and suppression are not technically accurate. However, these terms used in this circumstance have a history in the barn owl literature (Takahashi and Konishi 1986) and so will be used here as well, with the foregoing caveat.

The so-called "best" value of a given parameter was defined as the value which elicited the largest response. In some cases, the weighted average of the points surrounding the maximum response was used to interpolate the best value with greater precision. For the small number of sigmoid-shaped IID tuning curves, the best IID was taken as the point where the response just saturated.

Summary plots were made by shifting the x-axis to align some predetermined point, scaling the y-axis by the response to some predetermined stimulus, and then averaging across all neurons. For example, the two-tone frequency tuning curves of Figure 3.2 were shifted so that the fixed tones overlapped in frequency, and then scaled by the response to the fixed tone. These methods dealt much better with noise than the usual method of parameterizing each figure and then reporting statistics on those parameters.

Except where noted all error bars in both figures and text indicate the standard error of the mean. To improve clarity, the error bars in some figures have been averaged and plotted separately in the corner. Horizontal dotted lines indicate the spontaneous spiking rate unless redefined in figure legends.

The width data of Figure 4.5 were computed by dividing the area between the curve and the spontaneous rate by the maximum height of the curve. For noisy curves this formula is a much more robust estimator of the width than the more commonly used width at half height. Although it underestimates the width at half height by 6% for Gaussian curves, it yields identical results for triangular- or quadrilateral-shaped tuning curves.

The positions of fluorescent cells photographed at high-power (10-40x) were documented by taking low-power (2.5-5x) darkfield pictures without moving the stage. Nearby air bubbles were used to adjust for small translational differences between different objectives. The grayscale pictures from the microscope were artificially colored either red or green depending on the laser and filter chosen, and a montage was superimposed on a low-power darkfield image of IC. Somal area statistics were computed from a set of optical sections taken at 100x. Sections were taken at intervals equal to the section thickness (about 6 μm at this magnification) and then digitally flattened to reveal the largest extent of the neuron across all depths. Scalebars were measured with a calibration grid (Microbrightfield).

Chapter 3 Frequency convergence and the resolution of phase ambiguity in space-specific neurons

3.1 Introduction

Both humans and barn owls are more adept at localizing broadband noise stimuli than tonal stimuli (Butler 1986; Chandler and Grantham 1992; Knudsen and Konishi 1979; Bala and Takahashi 2000). In barn owls, this difference in acuity is due to a phenomenon called phase ambiguity (Saberi *et al*. 1998; Saberi *et al*. 1999), which arises from the way in which the peripheral auditory system encodes temporal information (Sullivan and Konishi 1984; Köppl 1997). Auditory nerve fibers are narrowly tuned to frequency and their spikes are locked to a particular phase angle. Hence, although interaural time difference (ITD) is the principal cue used to localize sounds in the horizontal plane (Moiseff and Konishi 1981), auditory nerve fibers only encode phase and so have spatially ambiguous responses. Only when information is combined across multiple frequencies is a sensitivity to phase difference converted into a sensitivity to time difference (Takahashi and Konishi 1986). This explains why behavioral acuity is better for noise stimuli, compared to tonal stimuli.

Takahashi and Konishi (1986) were the first to study the neural mechanisms of spectral integration in the barn owl. They recorded from the space-mapped neurons in the external nucleus of the inferior colliculus (ICx). For a free-field noise stimulus, neurons in ICx have spatially-limited receptive fields (Knudsen and Konishi 1978a). Correspondingly, ITD tuning curves taken with dichotic noise stimuli have a large peak at the ITD which encodes this receptive field (Takahashi and Konishi 1986).

Flanking this main peak, however, are smaller so-called side peaks, which are due to the phase-locked encoding scheme used in the periphery. Interestingly, pure-tone ITD tuning curves in ICx are phase ambiguous: all the peaks are of equal height. Takahashi and Konishi (1986) reported that roughly one third of the main peaks were facilitated and roughly one third of the side peaks were suppressed when the response to noise was compared with the response to a tone. These results can be explained through constructive and destructive interference: while at the ITD corresponding to the main peak, the pure-tone peaks are aligned across all frequencies, at the side peaks, they are all slightly misaligned because their spacing is inversely proportional to the stimulus frequency. This difference in alignment leads to the main peak being larger than the side peaks, which is what underlies the heightened behavioral acuity observed for noise stimuli.

The aim of the present study is to elucidate how the individual tones within a noise stimulus interact to resolve phase ambiguity. Collectively, we know that the interaction is facilitative at the main peak, and suppressive at the side peaks. But as of yet, no systematic relationship has been found between the type of interaction observed and the specific frequencies chosen in a two-tone stimulus. The data presented here show that such a relationship exists and demonstrate that the resolution of phase ambiguity is *not* dependent on the interactions between tones of nearby frequencies.

3.2 Results

Recordings were made from 79 well-isolated neurons in the external nucleus of the inferior colliculus (ICx). Due to time constraints, not all protocols were collected for each neuron. The number of neurons for each protocol is indicated in the appropriate section of the text and its associated figures. In most cases, each stimulus was repeated ten times. Except where noted, stimuli were played 20 dB above the threshold for noise at the interaural time (ITD) and intensity (IID) differences eliciting the maximum response, the so-called best ITDs and IIDs.

ICx was identified on the basis of stereotaxic coordinates and physiological response characteristics, and recording locations were confirmed with standard histological methods. Because the medial border of ICx with the lateral shell of the inferior colliculus is not well-defined physiologically or histologically, an arbitrary criterion of side peaks being at least 30% smaller than main peaks was used to identify the space-specific cells of ICx. Some cells were histologically identified to be in the deep layers of OT. Although these data showed results similar to ICx cells, they were excluded from the analysis presented below.

Noise versus best frequency ITD tuning curves

The characteristic feature of ITD tuning curves taken in ICx with noise stimuli is that there is one large peak (the main peak) surrounded by smaller peaks (the side peaks). For pure-tone stimuli the peaks are all of equal height (Takahashi and Konishi 1986). Figure 3.1 reconfirms this. Interleaved ITD tuning curves were taken with noise and BF stimuli for 46 neurons. The left panel shows an example response to noise (solid) and a pure tone at the best frequency (BF; dashed). In this case, the response to noise at the main peak was much greater than that to BF, a phenomenon called main-peak facilitation (MPF). While the left side peak was smaller for noise (side-peak suppression, SPS), the right one was roughly the same. The right panel shows a summary of 45 neurons. One neuron, which showed 4050% MPF, was considered an outlier and excluded. This figure was created by shifting the x-axis of each curve until the main peak of the noise response was at 0 μs, scaling the x-axis by 1/BF so that the side peaks were all aligned at 1 cycle, scaling the y-axis by the response to BF at the main peak, and then taking the mean across all neurons. On average there was 193% MPF and 13% side-peak *facilitation* (SPF; for the two side peaks immediately adjacent to the main peak). Table 3.1 discretely categorizes these data. While the majority (37/46) of main peaks showed facilitation, the majority (46/92) of side peaks did not change. The 19 side peaks which showed suppression were balanced by 27 which showed facilitation. These figures make it clear that although SPS can play a

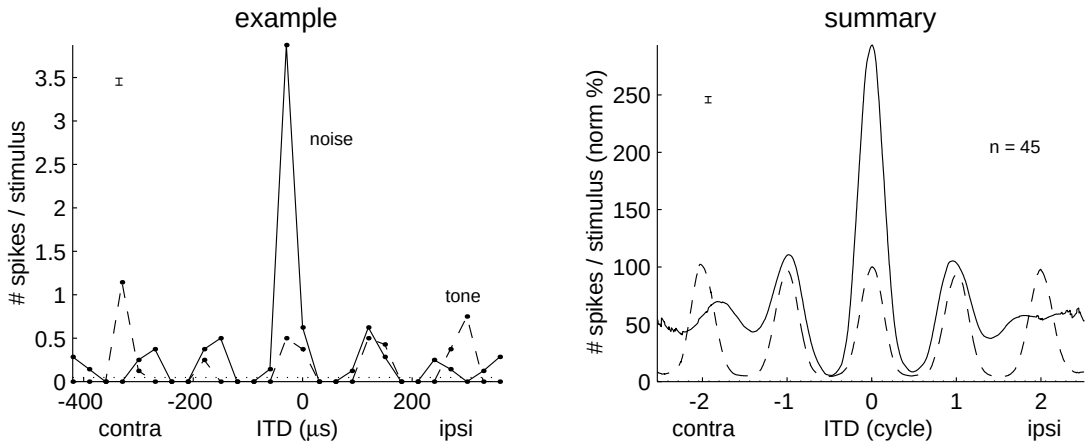

Figure 3.1: ITD tuning curves to broadband noise (solid) and a pure tone at the best frequency (BF; dashed). The dotted line indicates the spontaneous rate. (left) A specific example (owl 660; neuron 23). (right) A summary of 45 neurons, formed by shifting the x-axis so that the main peaks lined up, scaling the x-axis so that the side peaks lined up, normalizing the y-axis by the response to BF at the main peak, and then taking the mean. On average, the main peak was facilitated by 193% and the side peaks were *facilitated* by 13%. The single error bar in the upper left of each graph represents the average size of the standard error of the mean across all the data points. Noise and BF curves were interleaved for each neuron.

role in making the side peaks smaller than the main peaks, the dominant factor is main-peak facilitation.

One thing to note about these data is that the intensities of both noise and tonal stimuli are normalized such that the overall RMS amplitudes are identical. As described in *Methods - Analysis*, this causes the power of the individual tones within the noise stimulus to be quieter than when played alone. Strictly speaking, then, the terms facilitative and suppressive are not accurate when comparing these noise and tonal stimuli, for the tone played alone is not identical to the tone embedded in the noise. Nevertheless, the conclusion that phase ambiguity is resolved through main-peak facilitation is likely still valid, for if the stimuli were normalized appropriately, then the overall intensity of the noise would be much greater. And as rate-intensity curves for these neurons are generally sigmoidally shaped, a louder intensity would yield even more spikes, and hence result in even more facilitation.

noise re BF tone	main peak	side peaks
facilitation	37	27
equal	8	46
suppression	1	19

Table 3.1: Resolution of phase ambiguity. Indicated are the total number of main and side peaks from 46 neurons which show facilitation, suppression, or neither. The sum of the second column is twice as high as the first because there are two side peaks for each main peak.

Two-tone frequency tuning curves

To more precisely elucidate the role of spectral integration in the resolution of phase ambiguity, two-tone frequency tuning curves were taken in which one frequency was held fixed at the BF and the second varied in frequency. Figure 3.2 shows both exemplar and summary data at the main peak. The top left panel is a normal one-tone frequency tuning curve. The bottom left shows a two-tone frequency tuning curve (solid) that was taken interleaved with the normal one-tone frequency tuning curve in the upper left. The fixed tone was the BF, whose response when played alone is indicated by the large solid circle. There is a prominent lack of facilitation for probe tones near the fixed tone, with regions of facilitation on both sides. The dashed line is the response predicted from a linear combination of the two tones played separately. The difference between the solid and dashed lines is a measure of linearity and is shown in the upper right panel. The facilitation seen in the lower left panel is super-linear for probe tone frequencies distant from the fixed tone and sub-linear for probe tones near the fixed tone. (See *Methods - Analysis* for detailed definitions of suppression, facilitation, and sub- and super-linear.) The lower right panel shows the summary data corresponding to the upper right panel for 31 neurons. The x-axis of the plot for each neuron was shifted until the fixed tones were aligned at zero, the y-axis scaled by the response to the fixed tone presented alone, and then the data were averaged. The summary figure shows that the trends seen in the example figure are consistent across the data set: as the probe tone frequency moves further away

from the fixed tone, the response goes from extremely sub-linear to slightly super-linear to exactly-linear. The exactly-linear response can be explained by the probe tone frequency being outside the input frequency range of the neuron. Mechanisms for the sub-linear response for probe tones near the fixed tone are addressed in the *Discussion*.

Habituation-free two-tone tuning curves

One criticism of the two-tone frequency tuning curve data is that the protocol is subject to habituation. On average every other stimulus contains the fixed tone and so it's not unreasonable to expect that the neuron might habituate to it. In fact, this does occur, as shown in Figure 3.3. The right panel shows that there is a 10-15% decrease in the response to frequencies near the fixed tone for normal frequency tuning curves interleaved with two-tone frequency tuning curves, compared to normal frequency tuning curves that were not interleaved. This habituation is disturbing, for it could be argued that the prominent sub-linear notch in the interaction between two tones (Fig. 3.2, lower right) is simply an artifact of habituation. This explanation is unlikely, however, because the results presented in the lower right panel of Figure 3.2 are the difference between two data sets that were interleaved. Any effects due to the habituation should affect both data sets equally and should be canceled out in the difference. Nevertheless, a second protocol was devised which addressed the same question but did so in a way which avoided habituation. Specifically, a two-tone stimulus was again used, but this time neither tone was delivered at a fixed frequency. Rather, the two tones were moved symmetrically about the BF by holding the average frequency fixed at the BF and varying the difference between the frequencies. Habituation could not possibly be a problem as no frequency is repeated in each stimulus.

Figure 3.4 shows such habituation-free data taken at the main peak. The solid line in the upper left panel shows an example response to the two-tone stimulus as a function of the spacing between the tones. The dashed line shows the predicted

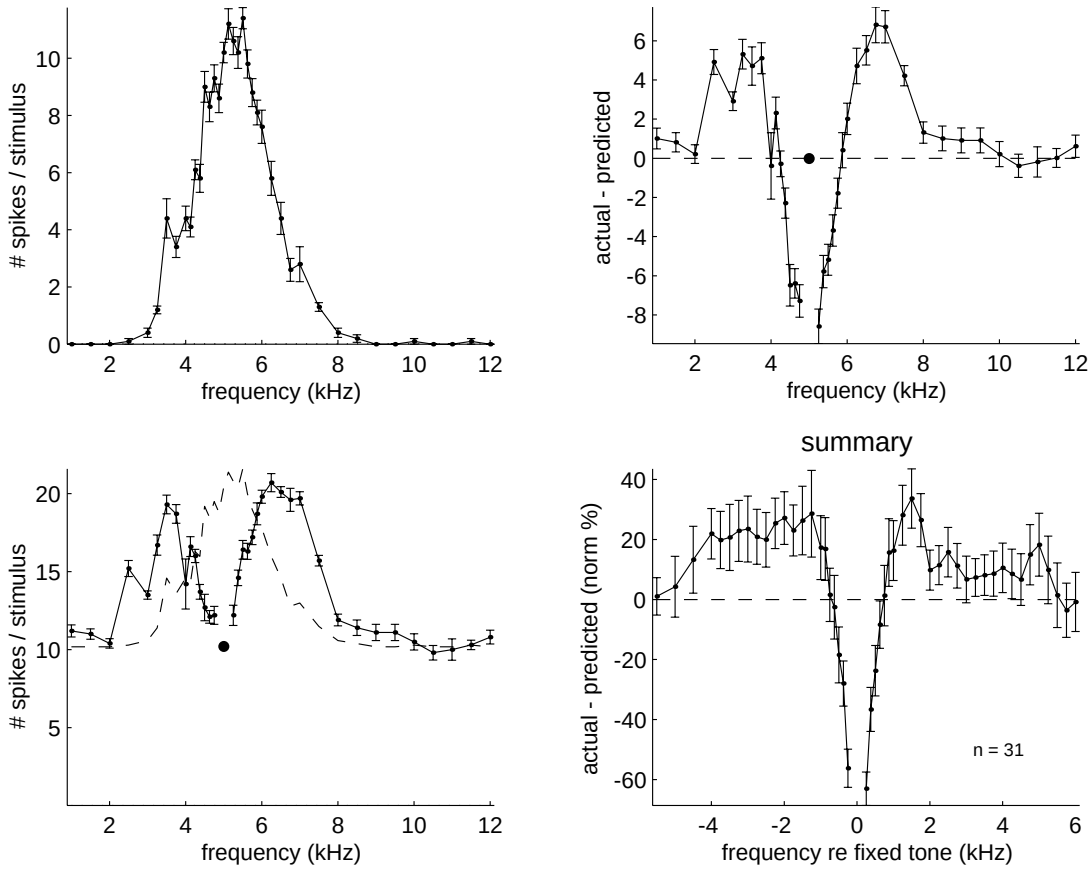

Figure 3.2: One- and two-tone frequency tuning curves. (upper left) A normal one-tone frequency tuning curve (owl 659, neuron 10). (lower left) The corresponding (i.e., from the same neuron) two-tone frequency tuning curve with the second tone fixed at 5000 Hz, the best frequency (BF). The dashed line is what is predicted from a linear combination of the responses to the two tones presented separately. Responses above the dashed line are super-linear, and below are sub-linear. The large solid circle represents the frequency of and response to the fixed tone presented alone. (upper right) The difference between the lines drawn in the lower left panel. The dashed line is an exactly-linear combination. Super- and sub-linear responses are above and below the dotted line, respectively. The large solid circle represents the frequency of the fixed tone presented alone. (lower right) A summary of upper-right-panel data from 31 neurons, formed by shifting the x-axis so that the frequency of the fixed tones lined up, scaling the y-axis by the response to the fixed tone presented alone, and then taking the mean. Note the transition from super- to sub-linear as the frequencies become closer together.

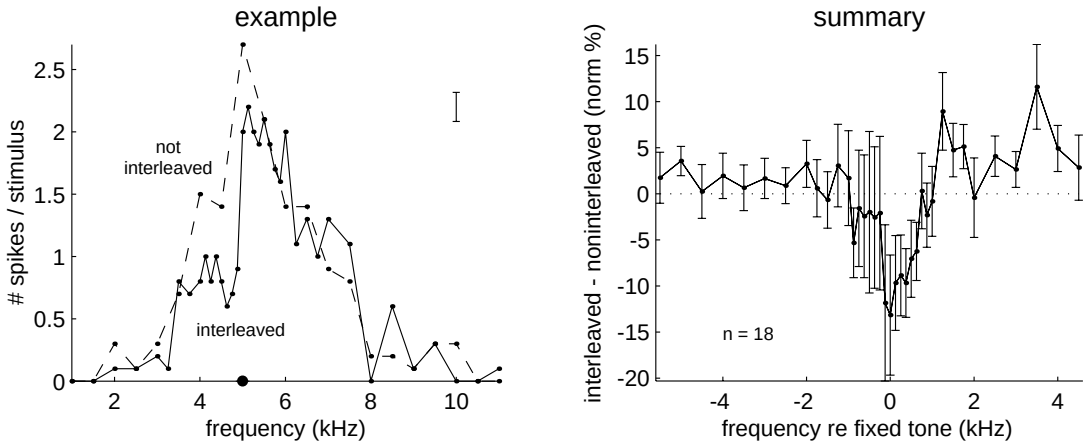

Figure 3.3: Habituation to repeated tones of the same frequency. (left) Two one-tone frequency tuning curves (owl 660, neuron 30), one of which was interleaved (solid) with a two-tone frequency tuning curve which had a fixed second tone of 5000 Hz (large solid circle), and the second which was not interleaved (dashed). (right) A summary of 18 neurons, formed by taking the difference between the two curves in the left panel, shifting the x-axis so that the frequency of the fixed tones lined up, scaling the y-axis by the response to the fixed tone presented alone, and then taking the mean. The dotted line indicates the interleaved and non-interleaved curves are identical. Note the drop in response near the frequency of the fixed tone.

response based on a linear combination of the responses to the two tones played separately. The difference between these two lines is a measure of linearity and is shown in the upper right panel. In this case, there is a transition from sub-linear to super-linear to exactly-linear as the separation between the tones is increased. The lower panels are the corresponding summary data for 32 neurons, formed by scaling the y-axis by the maximum response elicited by any of the frequencies presented alone, and then taking the average across all neurons. The summary data show that the trends seen in the example figure are consistent across the data set: the transition from sub-linear to super-linear is just less than 1 kHz.

So do the two-tone frequency tuning curve and habituation-free tuning curve protocols differ substantially in their results? Figure 3.5 directly compares the data. The solid line is identical to the lower right panel of Figure 3.2 and the dashed line to the lower right panel in Figure 3.4. The dashed line has been reflected about zero to

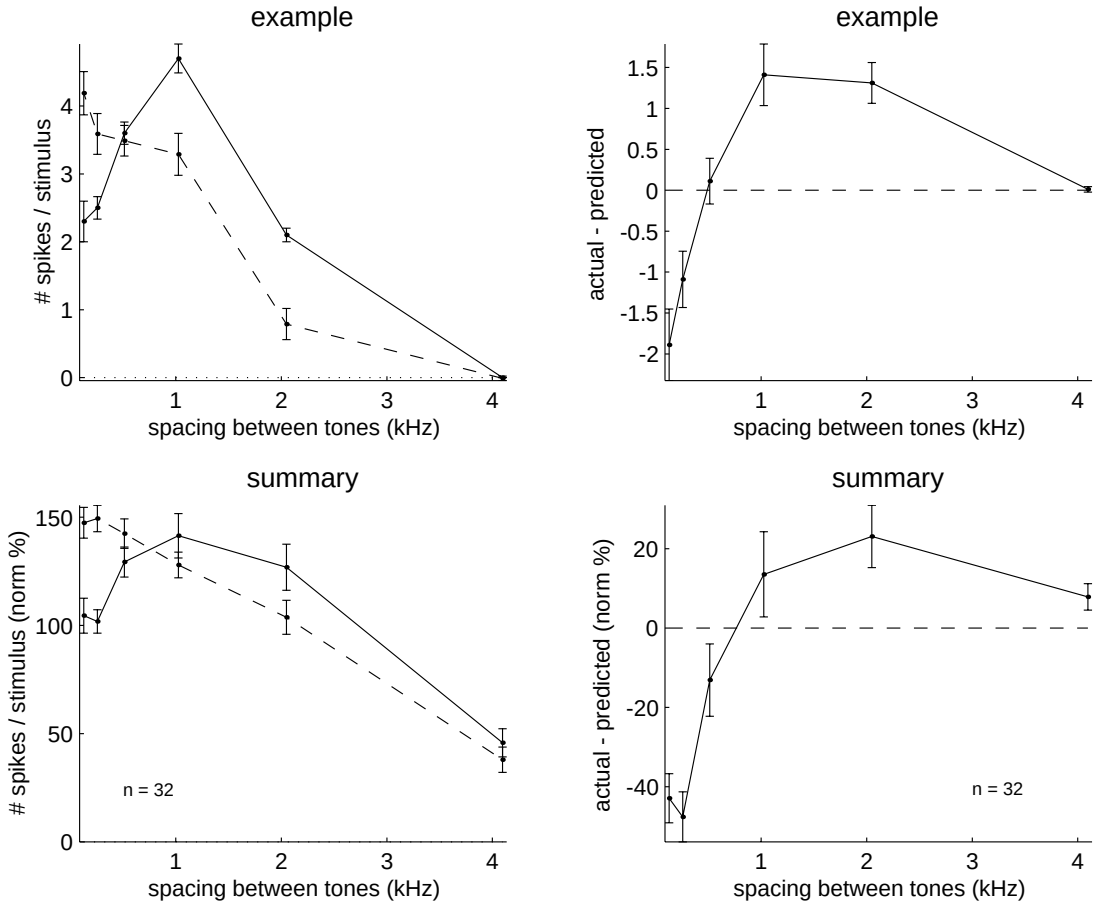

Figure 3.4: Two-tone frequency tuning curves with a moving second tone. The average frequency of the two tones was set to the best frequency of the neuron, while the difference between the two frequencies was varied. (left column) Actual (solid) responses to the two-tone stimulus and predicted (dashed) responses based on a linear combination of the two tones presented separately. (right column) The difference of the lines in the left column. The dashed line is an exactly-linear combination. Super- and sub-linear responses are above and below the line, respectively. (top row) A specific example (owl 660, neuron 2). (bottom row) A summary of 32 neurons, formed by normalizing the top-row data by the maximum response to a pure tone, and then taking the mean. Note the transition from super- to sub-linear as the frequencies become closer together.

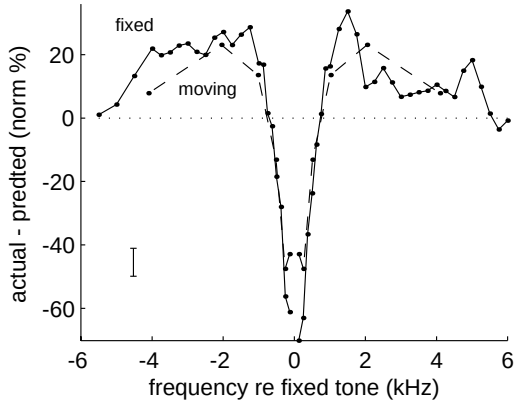

Figure 3.5: An overlay of the two-tone frequency tuning curve data with fixed (solid) and moving (dashed) second tones (i.e., the lower right panels of Figures 3.2 and 3.4, respectively). The moving two-tone data have been reflected about zero to show separations in both directions. The dotted line indicates an exactly-linear combination. The two protocols yield qualitatively similar results, and demonstrate that the sub-linear interaction between tones of nearby frequencies is not due to habituation.

show separations in both directions. With the exception of the two points closest to zero, the curves are not significantly different: both show a transition from sub-linear to super-linear for tones spaced just less than 1 kHz apart.

Sinusoidally amplitude-modulated noise

A second criticism of these two-tone frequency tuning curve data is that it might all be just an epiphenomenon of the beats produced when adding two tones together. The sum of two sinusoids of different frequencies is mathematically identical to a single sinusoid of the average frequency that is sinusoidally amplitude modulated at half the difference between the frequencies: $\cos\omega_1 t + \cos\omega_2 t = 2\cos\frac{1}{2}(\omega_1 - \omega_2)t \cos\frac{1}{2}(\omega_1 + \omega_2)t$. It could be that the prominent sub-linear interaction for two nearby frequencies is merely an artifact due to beats and is not indicative of how the system really integrates across frequencies.

To investigate this possibility, a protocol was devised to test the effect of beats independent of the spectral content of the stimulus. White noise was synthesized and then sinusoidally amplitude modulated at different frequencies with a 100% mod-

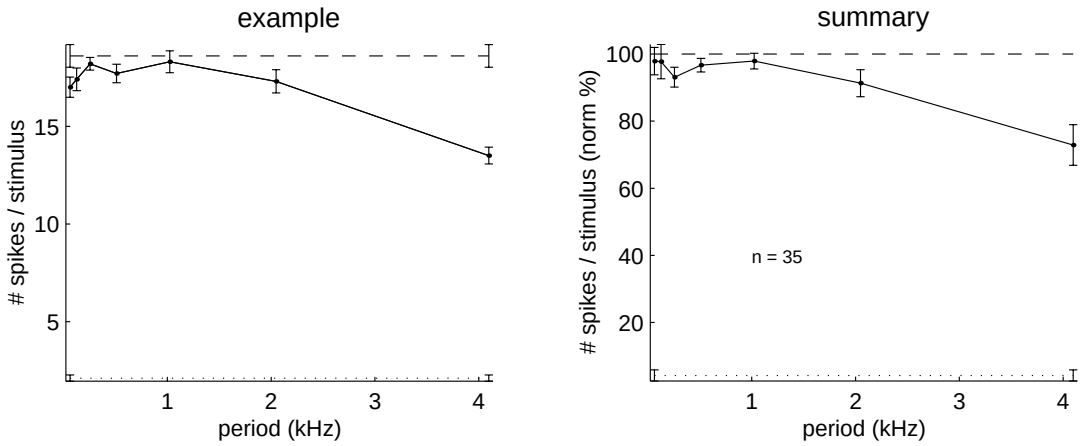

Figure 3.6: Responses to sinusoidally-amplitude-modulated noise (a.k.a. modulation-rate transfer function). (left) A specific example (owl 687, neuron 14). The dashed line is the response to unmodulated noise. (right) A summary of 35 neurons, formed by normalizing the y-axis by the response to unmodulated noise, and then taking the mean. Note that the response to modulated noise is not significantly different than that to unmodulated noise for slow periods, showing that the sub-linear interaction between tones of nearby frequencies is not due to beats.

ulation depth. The attenuators were adjusted so as to restore the intensity to its unmodulated value. Any difference in the response to these stimuli when compared to unmodulated noise could only be due to the beats. Figure 3.6 shows the results of this protocol for 35 neurons. In the left panel is an example. The response to the modulated noise is plotted against the frequency of the modulation. The dashed line indicates the response to unmodulated noise. For low modulation frequencies, corresponding to tone pairs of nearby frequencies, the responses are not significantly different. As the frequency of the modulation increases, there is a drop in the response to the modulated noise. The right panel is the corresponding summary figure, formed by normalizing the y-axis by the response to the unmodulated noise and then taking the mean. The summary data show that the trends seen in the example figure are consistent across the data set: below 1-2 kHz there is no significant difference between the modulated and unmodulated stimuli.

These data show that the prominent sub-linear interaction for two nearby frequencies is not an artifact of the beats produced by the addition of two tones. Modulated

and unmodulated noise elicited identical neural responses for modulation frequencies corresponding to the region of sub-linear interaction. However, the drop in the response seen at higher modulation frequencies indicates that the two-tone data might be affected for large separations between the frequencies. This would not change the conclusions of the previous sections, though, because such a drop would only mean that the true degree of super-linearity seen at these separations would be even larger than what was observed.

Frequency tuning curves at the side peak

Two-tone frequency tuning curves were also taken at the side peaks. These data are of particular interest in regards to the resolution of phase ambiguity. Figure 3.7 shows summary data for the smaller of the two immediately adjacent side peaks for 29 neurons. For comparison, the corresponding main peak data from the lower right panel of Figure 3.2 have been overlayed. There are two noteworthy points here: one is that nearby frequencies interact sub-linearly at the side peaks in a manner almost identical to that at the main peak. This indicates that the underlying mechanism is independent of ITD and is perhaps of a very general nature. Second: the slightly super-linear interaction for disparate frequencies at the main peak is greatly reduced at the side peak. The reduction is great enough that the interaction is often sub-linear, particularly for frequencies lower than the fixed frequency. The consequences of this differential interaction are to make the main peak bigger and the side peaks smaller than they would have been with just a strictly linear combination alone, and hence serve to further resolve phase-ambiguity.

One possible mechanism for the super- versus sub-linear interaction at the main and side peaks, respectively, is related to the data of Takahashi and Konishi (1986). Their Figure 2a (see Volman and Konishi 1989 as well) shows how the spacing between the phase-ambiguous peaks of pure-tone ITD tuning curves is proportional to the inverse of the stimulus frequency, which results in a misalignment of the side peaks across frequencies. When two-tone frequency tuning curves are taken at an ITD

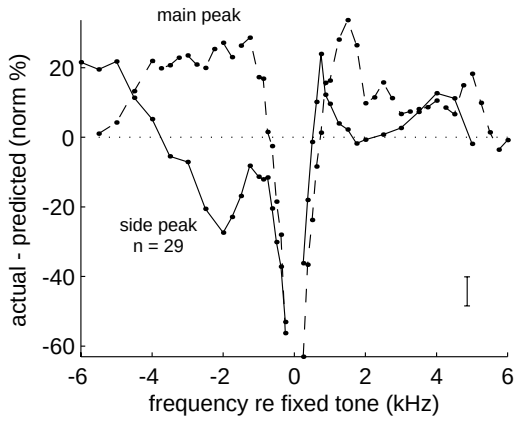

Figure 3.7: Two-tone frequency tuning curves at the side peak (solid) with the corresponding main peak data (dashed) of Figure 3.2 overlayed for comparison. The dotted line represents an exactly-linear combination. Note that tones of nearby frequencies interact sub-linearly at both the main and side peaks. Note also that tones of disparate frequencies interact more sub-linearly at the side peak than at the main peak, an effect consistent with the differing amounts of facilitation seen at the main and side peaks in response to broadband noise (Fig. 3.1).

corresponding to the side peak of the noise tuning curve, changes in frequency away from the BF will lead to the sampling of pure-tone ITD tuning curves at a point that is not at a peak, and perhaps in a trough. Such ITDs are termed "unfavorable" and the data of Figure 3.7 demonstrate that while pairs of frequencies which are both at favorable ITDs interact in a slightly super-linear manner (dashed), pairs in which one ITD is unfavorable interact in a slightly sub-linear manner (solid; unless of course the frequencies are sufficiently close so as to be in the sub-linear notch). This suggests that there might be distinct differences in the morphology and/or pharmacology of afferent inputs conveying favorable and unfavorable ITDs, a possibility which will be discussed in more detail in the *Discussion*.

Another consequence of the misalignment of side peaks in ITD tuning curves is that frequency tuning curves are narrower at the side peaks than they are at the main peak. Shown in Figure 3.8 are both exemplar and summary data of interleaved frequency tuning curves taken at the main and side peaks. The left panel shows a specific example in which the frequency tuning curve at the main peak (solid) was

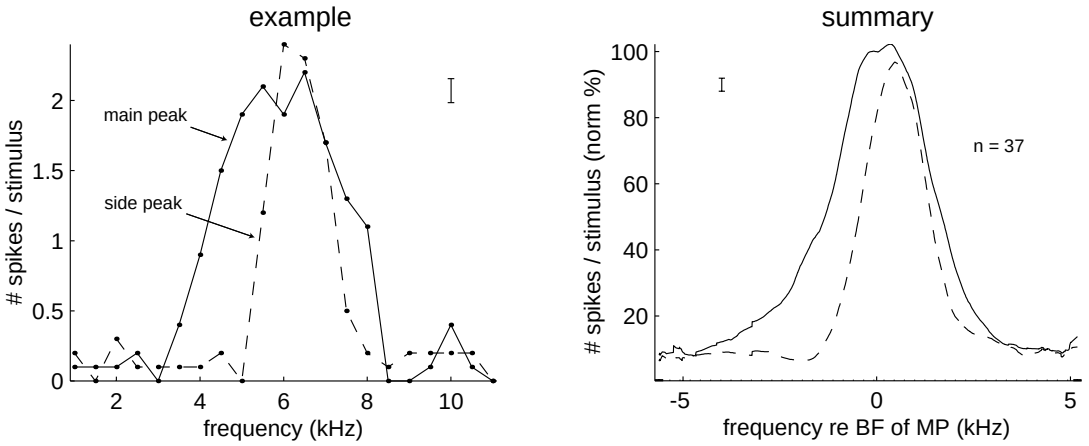

Figure 3.8: One-tone frequency tuning curves taken at ITDs corresponding to the main (solid) and side (dashed) peaks of noise ITD tuning curves. The ITDs of each curve were held fixed, despite the best ITD of the side peak changing with frequency. (left) A specific example (owl 687, neuron 10). (right) A summary of 37 neurons, formed by shifting the x-axis so that the best frequency (BF) of the main peaks lined up, normalizing the y-axis by the response to BF, and then taking the mean. Note that frequency tuning curves at the side peaks were narrower than those at the main peak, a result expected from the spacing of peaks in pure-tone ITD tuning curves changing with stimulus frequency.

3393 Hz wide at half height, while for the side peak (dashed) it was 1760 Hz wide. The right panel shows summary data for 37 neurons, formed by shifting the x-axis until the data taken at the main peak lined up, scaling the y-axis, and then taking the mean across all the neurons. On average, the widths were 1120 Hz narrower for the side peaks than the main peaks. This is significantly different ($p < 10^{-6}$). So while the resolution of phase ambiguity can be thought of as constructive and destructive interference of ITD tuning curves at different frequencies, a complementary and equally useful approach is to consider phase ambiguity to be resolved through a change in the bandwidth of spectral integration with ITD: main peaks are larger because a broader range of frequencies is allowed to facilitate each other than at the side peaks. This new approach in no way changes the model of how the system works, but rather provides us with a new way of looking at it.

N-tone stimuli

The data of Figures 3.2 and 3.7 both demonstrate that there is a prominent sub-linear interaction for tones of nearby frequencies. Figures 3.4 and 3.6 show that this interaction is not merely an artifact or epiphenomenon. To further characterize this interaction, two additional experiments were carried out. Specifically, they addressed the issue of how multiple tones interact to produce the facilitation seen with a noise stimulus at the main peak. Each involved using N-tone stimuli, with N being 2, 3, 5, 9, 17 or 33. In both cases, the distance in frequency between the outer-most tones was fixed at 4 kHz while the spacing between adjacent tones changed with N. The tones were always centered around BF and evenly spaced in frequency at a power-of-two multiple of 125 Hz.

Shown in the left two panels of Figure 3.9 are the data for which the intensity of the individual tones was kept constant, independent of N. This means that the overall intensity of the stimulus increases with N and allows actual responses to be compared to predicted responses. The top panel shows an example. The solid curve is the actual response to the N-tone stimulus and the dashed curve is what is predicted from the sum of the responses to the tones played individually. The response is linear for stimuli in which the adjacent tones are spaced 1 kHz or more apart, and sub-linear otherwise. The panel below shows summary data for 32 neurons, formed by scaling the y-axis by the maximum response to the N-tone stimulus and taking the mean across all the neurons. The boundary of 1 kHz between the exactly-linear and sub-linear responses is indicative of the entire data set.

Shown in the right two panels of Figure 3.9 are the data for which the overall intensity of the stimulus was kept constant, independent of N. This means that the intensity of the individual tones within the stimulus decreases with N and allows N-tone responses to be compared to noise. The top panel shows an example. The solid curve is the actual response to the N-tone stimulus and the dashed curve is the response to a noise stimulus of the same bandwidth and intensity. The response to the

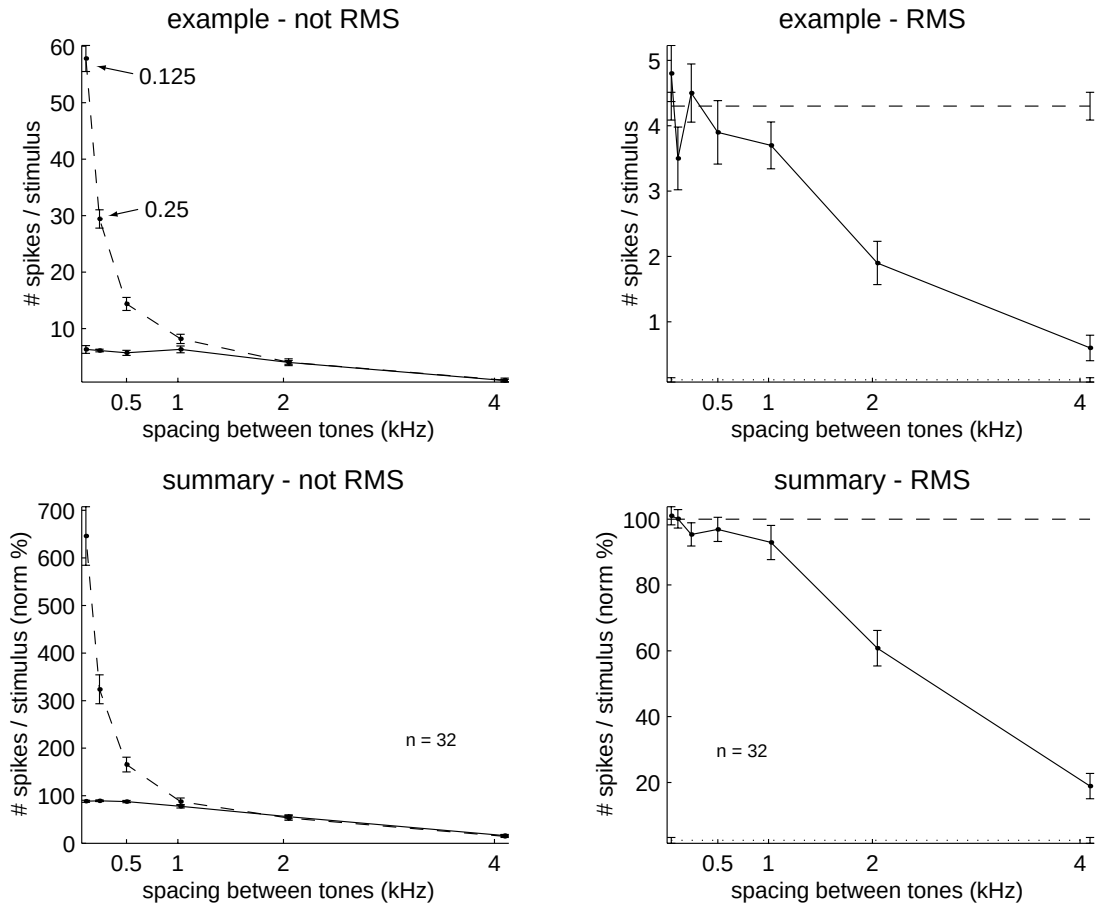

Figure 3.9: Responses to N-tone stimuli at the main peak. All stimuli had a fixed difference, or bandwidth, of 4 kHz between the smallest and largest frequencies. The independent variable was the number of tones, or equivalently, the spacing between adjacent tones, within that bandwidth. (upper left) A specific example of actual (solid) and predicted (dashed) responses to N-tone stimuli for which the amplitude of each frequency component was the same regardless of the number of tones (owl 676, neuron 15). Predicted responses were based on a linear combination of the tones presented separately. The amplitude of the entire stimulus was proportional to the log of the root of the number of tones, which created a 12 dB difference between the loudest and softest stimuli. (lower left) A summary of 32 neurons, formed by scaling the data by the maximum response elicited by any stimulus and then taking the mean. Note that the response is sub-linear for stimuli with adjacent tones less than 1 kHz apart. (upper right) A specific example of responses to N-tone stimuli in which the intensity of the stimulus as a whole was kept the same regardless of the number of constituent tones (owl 660, neuron 28). The dashed line indicates the response to noise of the same bandwidth. (lower right) A summary of 32 neurons, formed by scaling the data by the response to noise and then taking the mean. Note that the response to the N-tone stimulus is not significantly different from that to noise for stimuli with adjacent tones spaced less than 1 kHz apart.

N-tone stimulus is not significantly different than that to noise for stimuli in which the adjacent tones are spaced 1 kHz or less apart. The panel below shows summary data for 32 neurons, formed by scaling the y-axis by the response to noise and taking the mean across all the neurons. On average, N-tone stimuli with a spacing of 1 kHz or less elicit responses that are not significantly different than those elicited by noise.

These data provide further evidence that there is something special about the way space-mapped neurons, and perhaps the auditory system in general, integrates information spectrally. Not only do two tones interact sub-linearly when spaced less than 1 kHz apart (Fig. 3.2), but N-tone stimuli also interact sub-linearly when the adjacent tones are spaced less than 1 kHz apart (Fig. 3.9, left). Furthermore, N-tone stimuli are indistinguishable from noise so long as adjacent tones are less than 1 kHz apart (Fig. 3.9, right). In effect then, these data show that the facilitation seen at the main peak (Fig. 3.1) is independent of the fine details of the distribution of energy in the stimulus. It does not matter whether the energy is continuously distributed throughout it, or if it is discretely clumped into 1 kHz wide bands; resolution of phase-ambiguity will occur so long as the stimulus is of sufficiently broad bandwidth. Potential mechanisms are described in the *Discussion*.

3.3 Discussion

Phase ambiguity is a phenomenon which arises from the physics of sound waves and causes errors in the localization of narrowband sounds for both humans (Butler 1986; Chandler and Grantham 1992) and barn owls (Knudsen and Konishi 1979; Bala and Takahashi 2000). As has been well established, phase ambiguity is resolved (i.e., sound localization acuity is at its best) in the presence of the additional spectral information contained in broadband sounds (Saberi *et al*. 1998; Saberi *et al*. 1999). In the barn owl the neural underpinnings of the resolution of phase ambiguity involve facilitory and suppressive interactions between frequencies which augment the neural activity corresponding to a particular direction in space (Takahashi and Konishi 1986). These

interactions occur in the external nucleus of the inferior colliculus (ICx), where interaural time differences (ITDs) are used to create space-specific neurons arranged into a map of auditory space (Knudsen and Konishi 1978a). Figure 3.1 and Table 3.1 reconfirm these data and show that the difference between noise and puretone ITD tuning curves in ICx is almost entirely due to facilitation at the main peak. To avoid confusion regarding the underlying cause, this difference, frequently called side-peak suppression (SPS; e.g., Albeck 1997; Proctor and Konishi 1997; Mori 1997; Mazer 1998), will be referred to here as the main-peak to side-peak ratio (MSR; similar to M-SP difference in Peña and Konishi 2000). While these data qualitatively agree with Mazer (1998), who reported that either main-peak facilitation (MPF) or side-peak suppression (SPS) or both can occur to increase MSR, it is quantitatively different from Takahashi and Konishi (1986), who reported 36% of their neurons showed MPF and 28% showed SPS. In the sample presented here, the numbers were 80% and 21%, respectively (Table 3.1). Possible explanations for the differences between these two studies include the protocol used for anaesthesia, the criteria for accepting recordings for analysis, and the particular subset of neurons sampled. More interesting, however, is that 29% of the neurons in this sample showed side-peak *facilitation*. This statistic was not reported by Takahashi and Konishi (1986) and is generally not considered in more recent literature. 29% is roughly the same magnitude as the 21% which showed SPS, and explains why the overall difference in response at the side peaks between noise and pure-tone stimuli is small.

The individual frequencies within a noise stimulus interact in a systematic way. As shown with two-tone frequency tuning curves (Fig. 3.2, lower right and Fig. 3.4, lower right), there is a quite prominent sub-linear interaction for tones whose frequencies are less than 1 kHz apart. This interaction is not an artifact of habituation to the fixed tone (Fig. 3.3) or of beats between the tones (Fig. 3.6). There have been three other studies which have addressed this issue. Takahashi and Konishi (1986) took two-tone ITD tuning curves in ICx of the barn owl, but could not predict whether pairs of tones would elicit MPF or SPS based on the frequencies of the tones. This is probably due

to the limited number of frequencies they could sample with this lengthy stimulus protocol. The data presented here sampled more frequencies in less time by taking frequency tuning curves at the main and side peaks. Nelken *et al.* (1997) took two-tone frequency tuning curves in the dorsal cochlear nucleus of the cat. Their Figure 2D shows an exemplar neuron for which the interaction was sub-linear for tones of nearby frequencies and linear otherwise. Lu and Fay (1996) took two-tone frequency tuning curves in the auditory nerve and torus semicircularis of goldfish. Although their Figure 3 plots facilitation and suppression, instead of linearity (see *Methods - Analysis* for definitions), it is clear that they observed no sub-linear interaction for tones of nearby frequencies. This is probably due to the quiet intensity at which their stimuli were presented, a reason which will be clarified below.

The interaction between frequencies is also dependent on ITD. As shown with two-tone frequency tuning curves taken at the main and side peaks (Fig. 3.7), frequencies further than 1 kHz away from each other interact super-linearly at the main peak and sub-linearly at the side peak. This differential interaction serves to increase MSR in that it makes the main peaks bigger and the side peaks smaller than they would have been with just an exactly-linear convergence of frequencies alone. It also suggests that there might be differential morphology and/or pharmacology of afferent inputs conveying favorable and unfavorable ITDs. This idea has received considerable attention in the barn owl literature. Carr *et al.* (1989) stained the entire auditory system with antibodies to GAD and found GABAergic cells in both the central and external nuclei of the inferior colliculus. GABAergic cells were also found in the afferent lemniscal nuclei but not in the afferent cochlear nuclei. Feldman and Knudsen (1994) recorded from ICx and the lateral shell of the central nucleus of IC while simultaneously iontophoresing AP5 or CNQX and showed that glutamate receptors are largely of the NMDA type in ICx, while they are largely of the non-NMDA type in the lateral shell. Fujita and Konishi (1991) recorded from ICx while simultaneously iontophoresing BMI, a GABA-receptor antagonist, and found that phase ambiguity was increased. Mori (1997) also recorded from ICx while simultane-

ously iontophoresing BMI and used two-tone stimuli to show that non-linearities in ITD-tuning curves disappear with BMI. Most recently, Albeck (1997) and Peña and Konishi (2000), based on extracellular and intracellular physiological data from ICx, respectively, hypothesized that ITD-specific inhibition acts to selectively suppress the response at the side peaks relative to the main peak. All these studies, plus the new data presented here, support the idea that the convergence of frequencies in ICx is done in an ITD-dependent manner which enhances the reduction in phase-ambiguity.

One mechanism which might underlie a sub-linear interaction between tones of nearby frequencies is saturation of the afferent nuclei. ICx neurons are broadly tuned to frequency and receive information from multiple independent narrowly-tuned afferent neurons (Knudsen 1984). While two tones of disparate frequencies will excite different afferent neurons, tones of nearby frequencies will excite the same afferent neuron. Because the responses of these afferent neurons saturate for loud sounds (Sullivan and Konishi 1984; Peña *et al*. 1996), the total number of EPSPs from afferent neurons impinging on an ICx neuron might depend on the difference between the frequencies of a two-tone stimulus. For example, disparate frequencies which excite different afferent neurons might separately evoke 10 spikes each in two different afferent neurons and so elicit 20 EPSPs total in an ICx neuron. Played together they would also elicit 20 EPSPs total because these two afferent neurons are independent. But nearby frequencies would excite the same afferent neuron, and so while each tone might separately evoke 10 EPSPs in an ICx neuron, together they might only evoke 12 EPSPs because of the saturating response of the afferent neuron to intensity. This possibility could entirely account for the prominent sub-linear interaction seen in Figures 3.2, 3.4, and 3.7.

A second hypothesis attributes sub-linear interaction between tones of nearby frequencies to two-tone suppression at the level of the eighth nerve. When a second tone is played simultaneously with a fixed tone at an eighth nerve fiber's characteristic frequency (CF), the response can be less than what the CF tone elicits when played alone (Sachs and Kiang 1968). This phenomenon is called two-tone suppression. To elicit

suppression, probe tone intensities must exceed a certain threshold. This threshold is much greater than the intensity of the CF tone for probe tone frequencies distant from the CF, but decreases to become at or just below the CF-tone intensity for nearby frequencies (Abbas and Sachs 1976; Delgutte 1990). In the data presented above, probe tone and fixed tone intensities were always equal, so two-tone suppression in the eighth nerve would only come into play for two-tone stimuli of nearby frequencies. This is precisely where the prominent lack of facilitation is observed (see Fig. 3.2).

Convergence of information across frequencies has received much attention within the psychophysics community. One of the more studied behavioral phenomenon concerning frequency convergence is the critical bandwidth. This bandwidth, as first described by Fletcher (1940), is thought to reflect the range of frequencies across which auditory filters integrate information, and was discovered through experiments that measured the minimum bandwidth of noise necessary to mask an embedded tone of slightly louder intensity. Critical bandwidths are independent of the intensity of the tone, but exponentially related to its frequency. Interestingly, the proportionality constants are such that the intensity of a tone which is just masked by a noise is identical to the overall intensity of the portion of that noise within the critical band. This suggests that auditory filters simply integrate all the power within the critical bandwidth, ignoring the fine details of its distribution. Although critical bands are a behavioral phenomenon, many physiologists have used similar stimulus protocols to search for its neural underpinnings. Despite the controversy, there are data which suggest that while the exponential frequency dependence is determined in the cochlea (Ehret and Merzenich 1988; Moore *et al*. 1999), the intensity independence does not arise until the inferior colliculus (Ehret and Moffat 1984; Ehret and Merzenich 1985; Schreiner and Langner 1997).

The experiments presented here, while not specifically addressing critical bands, have discovered a phenomenon, sub-linear interaction between tones of nearby frequencies, which seems to be related. The distance in frequency space within which this sub-linear interaction occurs (Fig. 3.2) is roughly the same width as critical bands

(Dyson *et al*. 1998). Furthermore, the frequency spacing below which N-tone stimuli are indistinguishable from noise is also roughly the same as the critical bandwidth (Fig. 3.9). These data show that while the resolution of phase ambiguity is dependent on the bandwidth across which information is integrated, it is *not* dependent on the fine details of how the spectral energy in the stimulus is distributed locally. For auditory filters cause tones of nearby frequencies to interact sublinearly, which results in equal main-peak to side-peak ratios (MSR) for noise stimuli and N-tone stimuli, provided that the tone spacing does not exceed the critical bandwidth.

Chapter 4 Functional implications of the dependence of IID tuning on frequency in the barn owl

4.1 Introduction

There are two different approaches that are commonly taken towards models of the cues used to localize sound. One approach, referred to here as the parametric approach, defines specific cues and describes how these cues change with the direction of the source. Human psychophysicists have shown, for example, that interaural time and intensity differences (ITD and IID, respectively) are cues to azimuth and that monaural cues encode elevation (Middlebrooks and Green 1991; Blauert 1997). These rules (or, equivalently, this model) for how cues change are often expressed as mathematical equations and invariably have qualifications which specify under which conditions they are valid. So in humans ITD is proportional to the sine of the azimuth, but the proportionality constant is frequency dependent such that its value changes by 50% over the range of interest (Kuhn 1977). The benefit of the parametric approach is that it provides simple and useful rules of thumb for how cues change with the direction of a sound source.

The second approach to understanding sound localization cues is to not make simplifying rules at all, but rather to keep and use the raw data itself. These data, called head-related transfer functions (HRTFs), specify how the amplitude and phase for each frequency within a sound is transformed as it travels from the source to each ear. As such, they contain the frequency-specific values of both binaural and monaural cues for all directions in space. Moreover, because HRTFs do not make

any approximations, they are flexible enough to account for all directions in space, despite any non-linear interactions between ITD, IID, frequency, and direction. The parametric model is in essence just a set of mathematical equations fit to HRTF data. These equations are used to gain intuitive understanding of how the cues change with direction.

It is important to distinguish, however, between models of how cues change with the direction of a sound source, and models of how the system uses cues to compute the perceived direction of a sound. The parametric model leads one to believe that the system uses mathematical equations to convert ITD and IID into a direction in space: neural machinery takes the cues as variables in an equation and, along with fixed constants as parameters, evaluates the equation and outputs an azimuth and elevation. In contrast, the HRTF model suggests that frequency-specific cues are used as indices into a lookup table to compute direction: each row in the table contains vectors of ITD and IID versus frequency which correspond to a particular direction, and the neural machinery outputs the azimuth and elevation of whichever row matches the values of the frequency-specific cues in the stimulus. Though these two approaches will, by design, yield similar results, parametric models will in general deviate from HRTF models for some areas in their parameter space. These deviations provide a useful experimental paradigm by which these two computational models can be distinguished.

In this chapter, physiological experiments are described which address whether the parametric or HRTF model better describes the way in which the auditory space map is computed in the barn owl. The barn owl is an ideal species for such experiments because not only can it acutely localize sounds (Payne 1971; Konishi 1973), but there are also striking differences between the parametric and HRTF models of how cues change across auditory space (Moiseff 1989b; Keller *et al*. 1998). Unlike humans, the asymmetric ears of barn owls (Norberg 1977) cause IID to encode elevation, leaving only ITD to encode azimuth. While this parametric model of ITD is fairly accurate for not only all azimuths, but all frequencies and elevations as well, the relationship

between IID and elevation is nonmonotonic beyond 20 degrees of the horizontal plane. Moreover, IID encodes azimuth, as opposed to elevation, for frequencies below about 4 kHz. As a result, IID cues characteristic of a particular direction will change with frequency in a complex manner which is not accounted for by the traditional parametric model. Recordings from space-specific cells in the external nucleus of the inferior colliculus (ICx) presented herein quantify to what extent neural tuning to IID reflects this complex dependence on frequency, and hence address whether the computations leading to the space map use mathematical equations or lookup tables.

4.2 Results

Recordings were made from 50 well-isolated neurons in the external nucleus of the inferior colliculus (ICx). Due to time constraints, not all protocols were collected for each neuron. The number of neurons for each protocol is indicated in the appropriate section of the text and its associated figures. In most cases, each stimulus was repeated ten times. Except where noted, stimuli were played 20 dB above the threshold for noise at the interaural time (ITD) and intensity (IID) difference eliciting the maximum response, the so-called best ITDs and IIDs.

ICx was identified on the basis of stereotaxic coordinates and physiological response characteristics, and recording locations were confirmed with standard histological methods. Because the medial border of ICx with the lateral shell of the inferior colliculus is not well-defined physiologically or histologically, an arbitrary criterion of side peaks in ITD tuning curves being at least 30% smaller than main peaks was used to identify the space-specific cells of ICx. Some cells were histologically identified to be in the deep layers of OT. Although these data showed results similar to ICx cells, they were excluded from the analysis presented below.

Dependence of IID tuning on frequency

The head-related transfer function (HRTF) model of sound localization postulates that the space-specific neurons of ICx respond only when the patterns of the ITD and IID spectra in the stimulus match the spectra characteristic of the direction in space which a neuron encodes. This is distinct from the parametric model, in which ITD and IID are thought to be linearly equated with azimuth and elevation, respectively, and the spectral pattern of these cues is not used at all. The IID portion of these two models can be easily distinguished in barn owls because the asymmetry of their ears causes IID cues to be highly frequency dependent. For pure-tone stimuli the HRTF model would then predict that neural tuning to IID changes with frequency, whereas the parametric model predicts no such change at all. To test these predictions pure-tone IID tuning curves were taken from single ICx neurons to look for changes in IID tuning with frequency. The example of Figure 4.1 shows typical results. The upper left panel shows a frequency tuning curve and the other panels show five interleaved pure-tone IID tuning curves all from the same neuron. The IID eliciting the maximum response, the best IID, was +5.7 dB at 4.5 kHz, -2.2 dB at 5.5 kHz, -3.5 dB at 6.5 kHz, +0.5 dB at 7.5 kHz, and +2.5 dB at 8.5 kHz. The largest difference between best IIDs for any pair of frequencies was 9.2 dB between 4.5 kHz and 6.5 kHz. These data clearly support the HRTF model of sound localization, as only it predicts such changes in IID tuning with frequency.

More examples of the largest difference in best IIDs across frequencies for four neurons are shown in Figure 4.2. For each neuron three to six frequencies were chosen at which to take pure-tone IID tuning curves. The sampled frequencies were usually spaced about 1 kHz apart and usually included one or two frequencies on the flanks of the frequency tuning curve that elicited less than half the response at the best frequency. For each of four representative neurons, the data of Figure 4.2 show the two pure-tone IID tuning curves which had the most different best IIDs. Some neurons showed no differences at all (upper left), while others had bell-shaped tuning

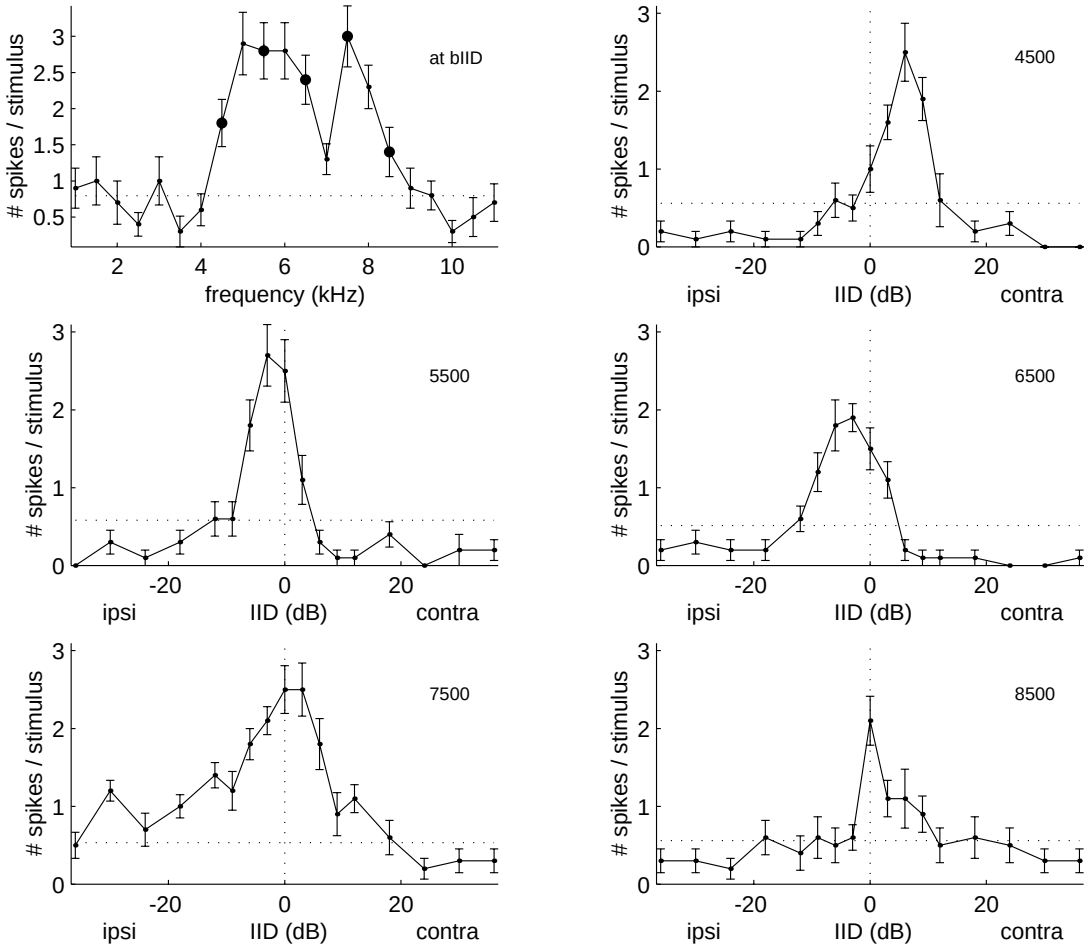

Figure 4.1: A frequency tuning curve (upper left), and five pure tone IID tuning curves all for a specific neuron (owl 687, neuron 17). Note the change in best IID from +5.7 dB at 4.5 kHz to -3.5 dB at 6.5 kHz. The frequency tuning curve was taken at the best ITD and IID, as determined with a broadband noise stimulus with the same ITD and IID for all frequencies. The pure tone IID tuning curves were taken in an interleaved fashion, at the frequencies indicated by the large solid circles. All stimuli were 20 dB above threshold. Vertical dotted lines indicate 0 dB IID. Horizontal dotted lines indicate spontaneous activity.

curves for some frequencies and sigmoid-shaped tuning curves for others (lower right). The latter case was infrequent, however, as of 210 pure-tone IID tuning curves, only 10 were sigmoidal. Most common were intermediate changes like those shown in the upper right and lower left panels: small shifts in the best IID of 3 to 12 dB with a substantial amount of overlap between the flanks of the curves.

Multiple pure-tone IID tuning curves were taken from a total of 50 neurons. Figure 4.3 plots the best IID versus frequency for each of these neurons separately. While frequency and IID tuning are linearly related in some neurons (e.g., owl 687, neuron 13, row 3, column 4), in other neurons the interaction is nonmonotonic (e.g., owl 691, neuron 9, row 10, column 3). In general there is no systematic relationship between best IID and frequency. Rather, it is assumed here that frequency-specific best IIDs match the IID spectrum characteristic of the location in space that this neuron encodes. Though this assumption was not verified with either free-field or virtual space stimuli in this study (c.f. Euston and Takahashi 2002), such a relationship is what would be predicted by the HRTF model.

To summarize the extent of the changes in IID tuning observed, a histogram of the largest differences in best IID is shown in Figure 4.4 (left). For each neuron the difference between the two frequency-specific best IIDs which were most different was computed and used as a measure of the effect of frequency on IID tuning. The average largest difference is 9.4 ± 6.2 (std. dev.) dB, which is significantly different than zero ($p < 10^{-13}$). For comparison, a histogram of the largest differences of the IID cue is shown in the right panel. These latter data were derived from the HRTF data of Keller *et al*. (1998) and span the region in space known to be mapped in ICx ($\pm 45^o$ azimuth, $+40^o$ to -60^o elevation, 4-8 kHz). The average largest difference in the IID cue of 14 ± 8.1 (std. dev.) dB is significantly larger than that of the neural data ($p < 10^{-4}$). Fortunately, this difference can be explained by two sampling biases: (1) frequencies were sampled discretely and so extreme best IIDs might be missed, and (2) a spatial fovea exists in the space map biasing our sample towards central locations where extreme IID cues are smaller. So while the changes in IID tuning are

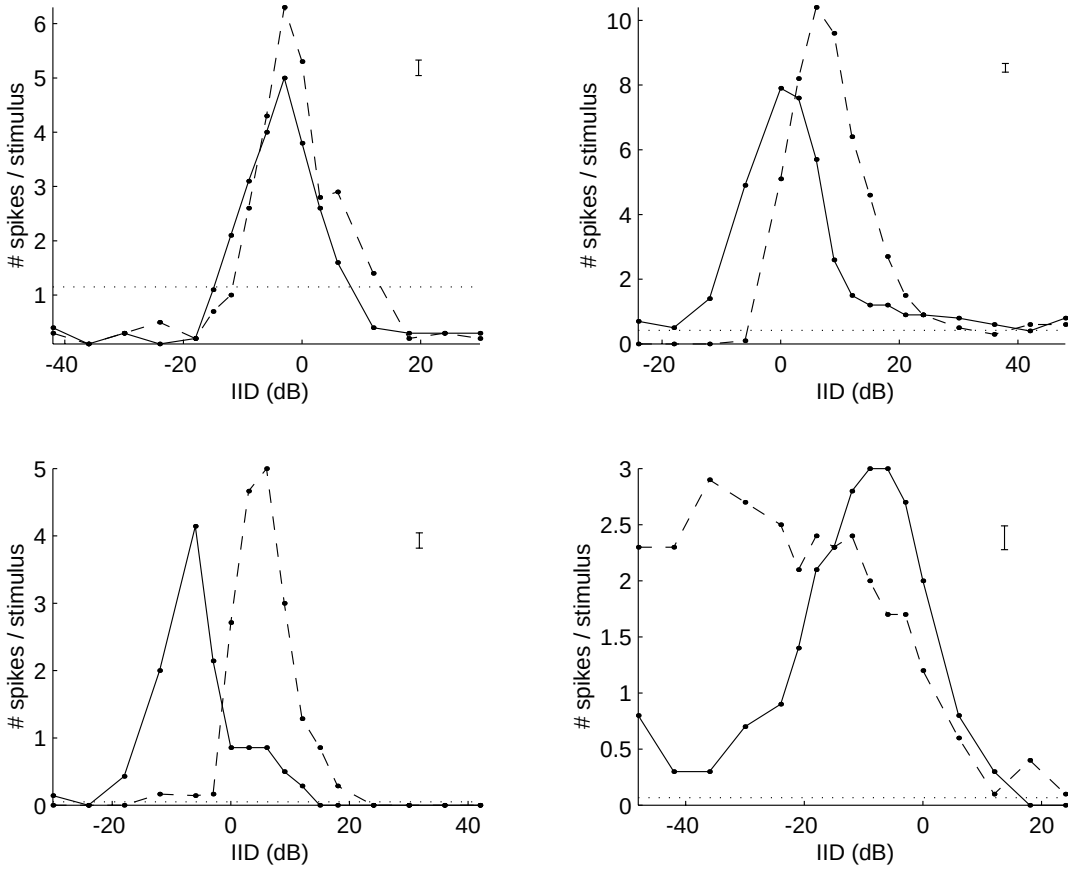

Figure 4.2: Examples from four different neurons of the largest observed changes in best IID with frequency. Solid and dashed lines each represent pure-tone IID tuning curves taken in an interleaved fashion at different frequencies. Three to six such pure-tone IID tuning curves were taken for each neuron, but only the two most different are shown here. The single error bar on the right of each graph represents the average size of the standard error of the mean across all the data points. (upper left) owl 687, neuron 6, 6.5 kHz (solid), 7.5 kHz (dashed). (upper right) owl 675, neuron 6, 6 kHz (solid), 7.5 kHz (dashed). (lower left) owl 676, neuron 14, 4.5 kHz (solid), 5.5 kHz (dashed). (lower right) owl 689, neuron 18, 5.5 kHz (solid), 7.5 kHz (dashed).

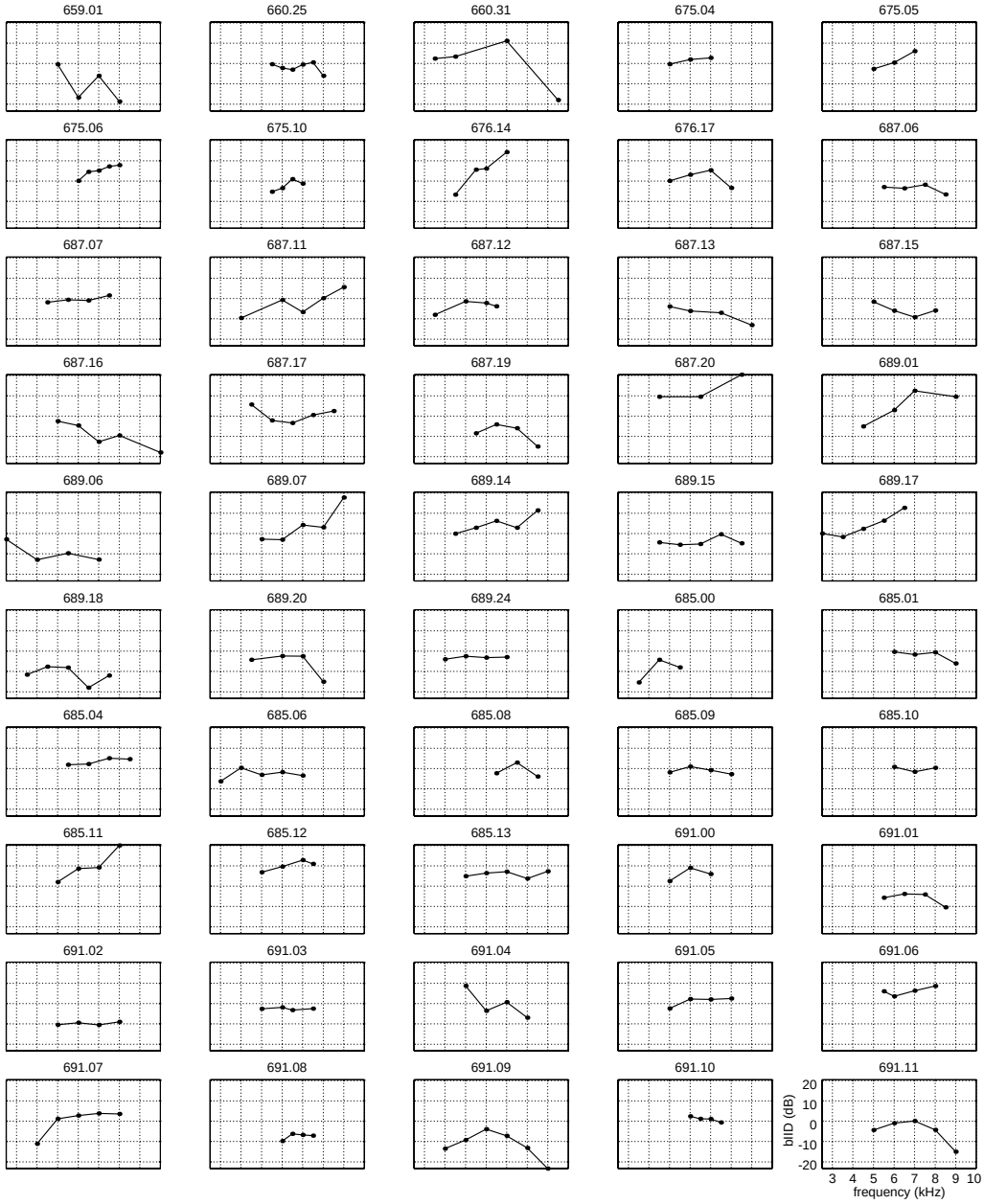

Figure 4.3: Graphs for all 50 neurons in this study for which best IID versus frequency data were obtained. There was no consistent relationship between best IID and frequency. All data for a given neuron was taken in an interleaved fashion. The scale of the grid lines is 10 dB and 1 kHz throughout, as indicated in the labelled graph in the lower right. Titles of each graph indicate the owl and neuron number.

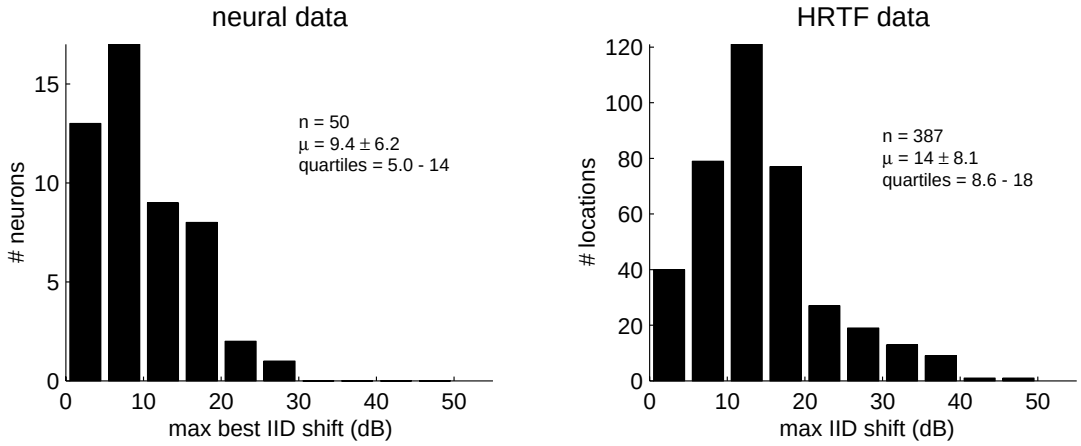

Figure 4.4: Histograms of the largest difference between best IIDs across frequency (left) and corresponding difference of head-related transfer function (HRTF)-IID cues (right; data courtesy of Keller *et al*. 1998). The magnitude of the observed differences in best IID with frequency were significantly smaller than expected from the HRTF data ($p < 10^{-4}$).

certainly significantly greater than zero, they are not quite as large as the HRTF data predicts. Yet one should not expect them to be that big either. Collectively, these data demonstrate a dependence of IID tuning on frequency, a result which favors the HRTF model of sound localization over the parametric model.

Responses to adaptive stimuli

The data of the previous section showed that IID tuning changes with frequency in the space-specific neurons of ICx. Given that HRTF data show that IID cues are frequency dependent for particular directions in space (Keller *et al*. 1998), it seems reasonable to think that these changes in IID tuning match the shape of the IID spectrum characteristic of the direction in space that the neuron encodes. Yet an equally striking characteristic of these data is the broadness of the width of pure-tone IID tuning curves. As shown in Figure 4.2, such broad widths cause there to be a substantial amount of overlap between IID tuning curves of different frequencies and moderate shifts in best IID. To quantify exactly how wide pure-tone IID tuning curves are, a histogram of the widths of the curves taken at the best frequency of each

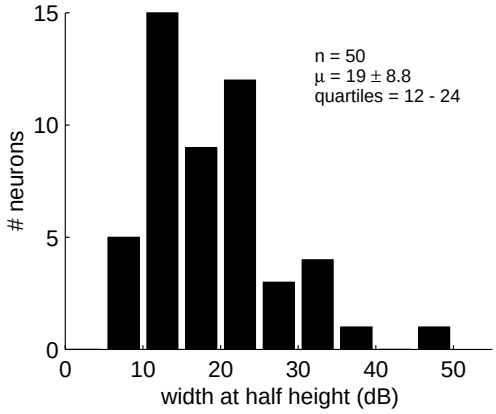

Figure 4.5: A histogram of the widths of the pure-tone IID tuning curves at the best frequency. The average width is about twice as large as the average of the largest changes in best IID with frequency (cf. Figure 4.4, left).

neuron is shown in Figure 4.5. The average width is 19 ± 8.8 (std. dev.) dB. This is about twice as large as the average of the largest differences in best IID (c.f. Fig. 4.4, left), which means that on average, IID curves of different frequencies will overlap by about half of their area. Because of this substantial overlap, one cannot be sure that a natural free-field stimulus would elicit a better response than a dichotic stimulus with a flat IID spectrum.

Three types of two-tone stimuli were used to address this issue. The idea was to compare the responses between normal flat-spectrum stimuli ("flat") and simulated free-field stimuli ("adaptive"). "Flat" two-tone stimuli had the same frequency-specific IID for both frequencies, each identical to the value on the abscissa. For "adaptive" stimuli, the frequency-specific IIDs were adjusted to match the previously determined best IIDs, and the abscissa indicates the deviation from the best IID. "Maladaptive" stimuli were similar to adaptive stimuli, but the frequency-specific IIDs were adjusted in the opposite direction.

An example of one neuron's response to these two-tone stimuli is shown in Figure 4.6. This neuron is the same neuron as shown in the upper right panel of Figure 4.2. For a 6 dB difference between the best IIDs of the two chosen frequencies, the adaptive stimulus (solid) elicits both a taller and narrower response than the flat

stimulus (long dashed). Similarly, the flat stimulus elicits a taller and narrower response than the maladaptive stimulus (short dashed). These data demonstrate that this ICx neuron is sensitive to the shape of spectral IID cues, and hence support the HRTF model of sound localization.

Figure 4.7 shows summary statistics across 31 neurons for which these data were collected. The average difference between best IIDs for this subset of data is 7.0 dB, somewhat smaller than the 9.4 dB observed for the entire data set of this study. The height, width, and ratios of height to width (i.e., Q values) were computed for each of the adaptive and maladaptive curves and then normalized by the corresponding values for the flat curve. Compared to flat stimuli, adaptive stimuli elicit significantly larger responses, though the widths and Q values are not significantly different. Heights, widths, and Qs are all significantly different when comparing flat to maladaptive stimuli.

There is a slight trend for pairs of frequencies with larger differences in best IID to elicit larger increases in spike rate for adaptive stimuli. Figure 4.8 plots the normalized height of the adaptive curve versus the difference in the best IID of the two frequencies for the same data set as Figure 4.7. The horizontal dashed line indicates the height of the flat curve. A linear regression line fit to the data (excluding the three outliers shown as Xs) shows a 17% increase in spike rate for every 10 dB difference in best IIDs. This trend is just barely significant ($p < 0.05$), however, and only 12% of the variance is accounted for by a linear fit. Nevertheless, these data collectively support the idea that ICx neurons respond best when the spectral IID cues match a preferred spectral shape.

Quantification of IID discrimination ability

The data of Figures 4.1 through 4.4 show that IID tuning changes with frequency. Figures 4.6 through 4.8 show that stimuli whose IID spectrum matches that which is assumed to be characteristic of the neuron's spatial direction elicit a larger response. To further characterize to what degree ICx neurons are sensitive to IID spectrum, one

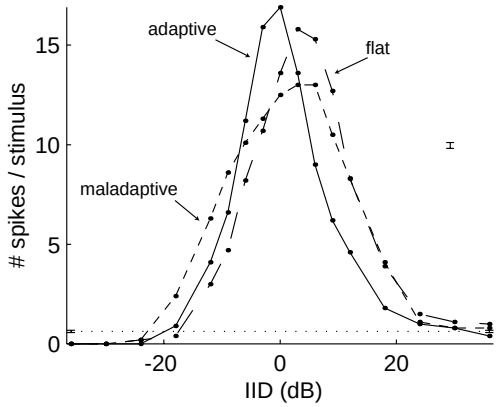

Figure 4.6: An example of two-tone IID tuning curves with adaptive (solid), flat (long dashed), and maladaptive (short dashed) stimuli. The adaptive curve is both taller and narrower than the flat curve, as is the flat curve relative to the maladaptive curve. Flat stimuli had the same frequency-specific IID for both frequencies, while for adaptive stimuli, the frequency-specific IIDs were adjusted to match the previously determined best IIDs. In this example (owl 675, neuron 6), 0 dB IID on the abscissa means an IID of 0 dB at both 6 kHz and 7.5 kHz for the flat stimulus, but 0 dB at 6 kHz and +6 dB IID at 7.5 kHz for the adaptive stimulus (see Figure 4.2, upper right). Maladaptive stimuli were similar to adaptive stimuli, but the frequency-specific IIDs were adjusted in the opposite direction. All three curves were taken in an interleaved fashion. Horizontal dotted line indicates spontaneous activity.

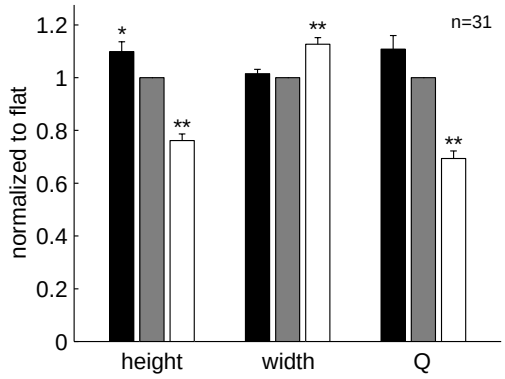

Figure 4.7: Summary data for the two-tone adaptive (black), flat (gray), and maladapative (white) stimuli for 41 pairs of frequencies taken from 31 neurons. The left triplet of bars shows the height of the IID tuning curves, the middle triplet shows the width, and the right shows the height divided by the width (a.k.a. Q). All data were first normalized to the response to the flat stimulus before taking the average. Error bars indicate standard error of the mean. Asterisks indicate a significantly different response compared to the corresponding flat stimulus (one asterisk means $p < 0.005$; two means $p < 0.0005$; none means $p > 0.1$; two-tailed paired Wilcoxon signed rank test).

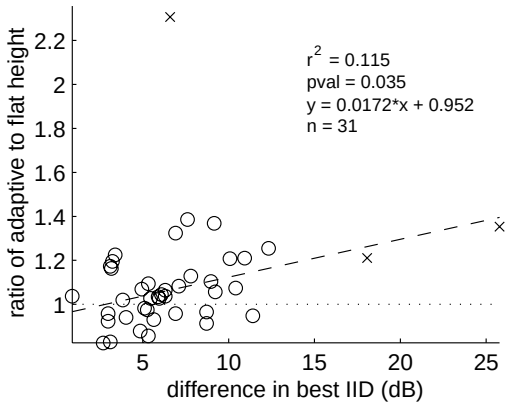

Figure 4.8: The change in the relative height of the responses to adaptive and flat two-tone stimuli as a function of the difference in best IIDs of the two frequencies. Horizontal dotted line indicates no change at all. Dashed line is a linear fit to the data, excluding the three outliers shown as Xs. Adaptive stimuli elicited on average 17% more spikes than flat stimuli for every 10 dB difference in best IID.

additional experiment was carried out. A two-tone stimulus was used again, but this time one frequency was fixed at its best IID while the second frequency was swept in IID. The idea was to see how close the IID of the swept frequency needed to be to its best IID to improve the response to the fixed tone. In effect, this last set of data creates a measure of distance in IID space. Such a measure is important to quantify, for it allows the similarity of two IID spectra to be judged, a task which the HRTF model of sound localization purports that ICx neurons perform.

Exemplar and summary data are shown in Figure 4.9. Two pure-tone IID tuning curves are shown in the top left panel. In the top right is the corresponding two-tone curve in which one of those tones was held fixed at its best IID while the other one was swept in IID. There is a central region where the swept tone facilitates the response to the fixed tone. Flanking the facilitation are regions of suppression on both sides. The bottom panel shows summary data for 33 neurons formed by shifting the x-axis of the top right panel data so that the peaks are aligned, scaling the y-axis by the response to the fixed tone presented alone, and then taking the mean across all neurons. The peak in the facilitory region is very sharp and elicits a response twice as big as the fixed tone presented alone. The transition from facilitation to suppression

occurs 16 dB from the maximal response. For some neurons the presence of the fixed tone also changed the best IID of the swept frequency. These changes were small, however, and not significant ($p > 0.6$).

Because the size of the facilitory region indicates how close a frequency-specific IID cue needs to be to its best IID to increase the overall response to the rest of the stimulus, the value of 16 dB can be taken as a measure of how close IID spectra need to be to match. Equivalently, this value can also be thought of as a measure of the ability of ICx neurons to discriminate IID. Yet 16 dB is certainly not indicative of their absolute sensitivity to IID, for the peak in the summary data of Figure 4.9 is very sharp, indicating that even small deviations from the best IID elicit less than maximal responses. The point where the interaction makes the transition from facilitation to suppression was chosen as a metric simply because it is the only non-arbitrary point on this curve.

4.3 Discussion

The use of interaural intensity difference cues (IID) by the barn owl for sound localization has traditionally been modeled as a simple linear function for the computation of elevation (Moiseff 1989a). Every 0.75 decibels of IID encoded a degree of elevation. The right ear louder meant the source was above the horizon, and left ear louder meant it was below the horizon. Recent measurements of head-related transfer functions (HRTFs; Keller *et al.* 1998), however, show that while there is indeed a linear relationship between IID and elevation for high-frequency sounds in the center of the frontal hemi-field, this relationship cannot be generalized to all frequencies and all locations. Specifically, there is a large dependence of IID on frequency. The dependence is non-monotonic and, moreover, the IID spectrum, as it is called, is highly dependent on the spatial location of the sound source. This spectral and spatial variance of IID is unique enough that the HRTF model of sound localization purports that the IID spectrum of the incoming stimulus is matched to the IID spectra characteristic of

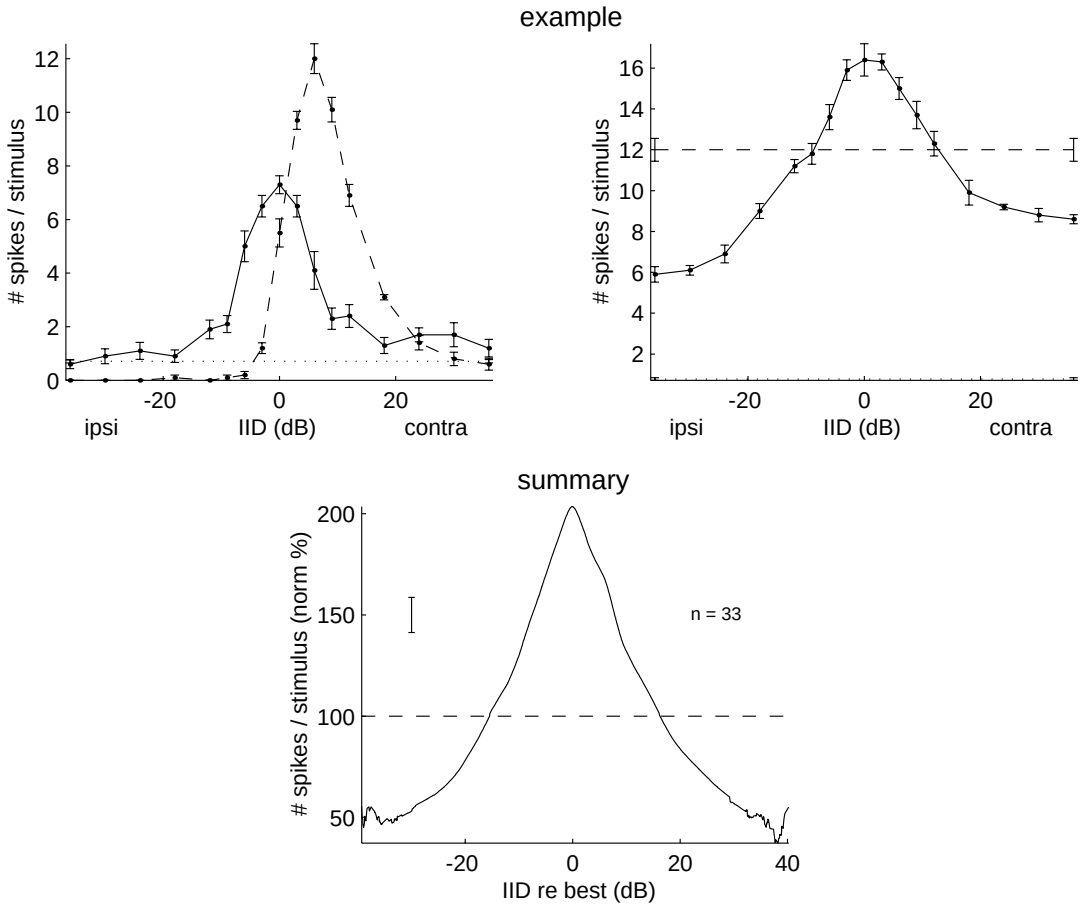

Figure 4.9: Two-tone IID tuning curves with one tone fixed at its best IID. A central facilitory region is flanked by suppressive regions. The sharpness of the peak serves as a measure of how close IID spectra need to be to match. (top) A specific example (owl 675, neuron 6). The top left graph shows two pure-tone IID tuning curves (6 kHz, solid; 7.5 kHz, dashed) with each frequency played separately. The top right graph shows a two-tone IID tuning curve with 7.5 kHz fixed at 6 dB and 6 kHz swept in IID. The horizontal dashed line indicates the response to 7.5 kHz at 6 dB played alone. Both pairs of curves were separately taken in an interleaved fashion. (bottom) An average of 65 such curves from 33 neurons. The transition from facilitation to suppression occurs 16 dB from the peak. The horizontal dashed line indicates the response to the fixed tone played alone.

locations in space. Whichever spectra matches the best is perceived as the location of the sound source.

The HRTF model of sound localization is distinctly different than the linear parametric model. Experiments presented here were specifically designed to discriminate between these two computational algorithms. The first such experiment involved taking pure-tone IID tuning curves from the space-specific neurons of the external nucleus of the inferior colliculus (ICx). The HRTF model predicts that such neurons will be tuned to different IIDs at different frequencies, with the shape of the relationship matching the shape of the IID spectrum characteristic for the neuron's spatial receptive field. The parametric model, on the other hand, has no concept of frequency-specific IIDs, and so does not predict any change in IID tuning with frequency. As the data of Figures 4.1, 4.2, 4.3, and 4.4 show, there are clear and obvious changes in IID tuning across frequency within single space-specific neurons.

A second experiment designed to distinguish between the HRTF and parametric models compared the neural responses between "adaptive" and "flat" stimuli. Adaptive stimuli had IID spectra which matched the spectrum assumed to be characteristic of the neuron's spatial receptive field, while "flat" stimuli had the same IID across all frequencies. The HRTF model predicts that better (i.e., taller and narrower) IID tuning curves will result from adaptive stimuli because the IID spectrum of that stimulus matches the characteristic IID spectrum better than the flat stimulus does. As the data of Figures 4.6, 4.7, and 4.8 show, adaptive stimuli do lead to better responses, though only the height of the tuning curves is significantly different. One limitation of this data set is that it does not include very many neurons which showed large differences in IID tuning. By chance such neurons were lost before this protocol was taken, making the average of the largest changes in IID tuning slightly smaller than this study's data set as a whole. Given that there was essentially no change in the width of the IID tuning curves between adaptive and flat stimuli, it seems likely that a data set whose changes in IID tuning were slightly larger would yield even larger improvements in IID tuning with adaptive stimuli.

There have been several other studies in barn owls concerning HRTFs. Moiseff (1989b), Olsen *et al.* (1989), Brainard *et al.* (1992), Keller *et al.* (1998), Euston and Takahashi (2002), and Poganiatz and Wagner (2001) have all measured HRTFs with microphones in the ears, and have all reported very similar results: IID changes with elevation for high-frequency sounds in the center, but for low frequencies it changes with azimuth, and in the periphery the relationship between IID and elevation is non-monotonic. Moiseff (1989b) used dichotic stimuli with flat IID spectra in awake behaving owls to show that changes in the overall IID elicited changes in the elevational component of the resulting head saccade. Keller *et al.* (1998), Euston and Takahashi (2002), and Poganiatz and Wagner (2001) used dichotic stimuli with HRTF-matched IID spectra to create a virtual sound source which elicited behavioral and physiological results identical to that of a real free-field sound source. Brainard *et al.* (1992) showed that spatial ambiguities with tones were resolved with noise. Gold and Knudsen (2000) and Euston and Takahashi (2002) were the first to show a dependence on frequency of IID tuning in space-specific neurons, a result confirmed and expanded upon in this study. And Egnor (2000) and Poganiatz and Wagner (2001), using modified virtual sound sources, both concluded that frequency-specific IID clues must play some role in localization, as overall IID can't explain all of the variance in the elevational component of head saccades. These last two studies are particularly important, for they provide the behavioral counterpart to the physiological data presented here, that IID spectrum is an important sound localization cue.

HRTFs have also been studied extensively in several mammalian species. Measurements have been made in the ferret (e.g., Carlile 1990), cat (e.g., Musicant *et al.* 1990), bat (e.g., Wotton *et al.* 1995), and human (reviewed by Blauert 1997). In symmetrically-eared species such as these, azimuth is thought to be encoded by IID for high frequencies and by ITD for low frequencies. Monaural and binaural spectral intensity cues are used to determine elevation, as well as to resolve front-back ambiguities due to the cone of confusion. Kuhn (1979) and Lawrence and Simmons (1982)

have shown that changes in the shape and/or position of the outer ear can result in large changes in the HRTFs. Interestingly, while Mills (1960), Hafter *et al.* (1977), and Yost and Dye (1988) have all shown that humans can discriminate IIDs as small as 1-2 dB, Kulkarni and Colburn (1998) have shown that the fine-structure of HRTFs is not important for localization ability. Nevertheless, Hirsch *et al.* (1985), Irvine and Gago (1990), and Mendelson and Grasse (2000) have all shown that IID tuning changes with frequency in the inferior and superior colliculi of cats. Moreover, Wise and Irvine (1985) have quantified IID-tuning widths in the cat superior colliculus and found them to average 25 dB.

Some modeling/theoretical work on HRTFs has been done as well. Neti *et al.* (1992), Datum *et al.* (1996), Chung *et al.* (2000), Gill *et al.* (2000), and Nandy and Ben-Arie (2001) have all trained back-propagation neural networks (Rumelhart *et al.* 1986) to localize using HRTF data. While the network architectures of these studies are all of similar design, the HRTF data used to train and test them varied from human, to cat, to a simulated pair of cardiod microphones. That similar sound localization performance levels can be achieved with such diverse HRTF data suggests that this approach is species independent: a neural network of identical architecture could be used for any species if it were just trained with the HRTF data of that species. This is a deep insight, for these models portray the neural computations underlying sound localization as the recognition of IID and ITD spectral patterns. Simplifying species-specific rules, such as IID encodes elevation and ITD encodes azimuth, were not used. Rather, the networks were just given the full HRTF data and trained to localize themselves.

Physiological data which address the use of pattern recognition to localize sounds is given here in Figure 4.9. Essentially, what the neural network models do is match the incoming IID and ITD spectra of the stimulus to spectra characteristic of particular directions in space. Hence, it would be nice to quantify the precision with which space-mapped neurons can discriminate spectral patterns. In the barn owl, the IID cue lends itself to such analysis because it is very strongly dependent on frequency.

Two-tone stimuli were used in this study to quantify IID spectrum discrimination, in which one frequency was held fixed at the best IID and the second varied in IID. The data (see Figure 4.9) show that there is a region of IIDs for which the second tone facilitates the response to the fixed tone, flanked by regions in which the interaction is suppressive. The width of the facilitatory region and the sharpness of the peak can be used as a measure of how close IID spectral patterns need to be to their characteristic IID pattern to match. Because the facilitory region is of non-zero width, it corroborates the data of Kulkarni and Colburn (1998) that the fine-details in the HRTF don't matter.

Gold and Knudsen (2000) provide further evidence that pattern recognition is used by the owl to localize sounds. They report that owls raised with permanently-implanted devices which alter their HRTFs localize sounds just as well as normal owls. Recordings from space-mapped neurons in these owls show frequency-specific changes in both IID and ITD tuning which match the characteristics of the implanted device. Seemingly, the innate pattern of the projections from the frequency-specific maps of IID and ITD in the brainstem to the auditory space map in the midbrain can be modified to match the HRTFs the owl experiences while developing. In other words, it appears as if juvenile owls, much like neural networks, have the ability to learn an arbitrary set of HRTFs.

In summary, while parametric models of sound localization cues which make species-specific simplifications can be useful in understanding how the values of those cues change with location, neurophysiological data show that the computation of sound location is actually being done by a pattern recognition algorithm. In the barn owl, the parametric model of the IID cue is good for ± 20 degrees in elevation, yet the neural space map extends from +40 to -60 degrees in elevation. For this extended range, HRTFs not only more accurately represent the available cues, but are also more indicative of the underlying neural computations. It is better, then, to think of space-specific neurons as pattern recognizers, as this not only accounts for all of the space map in the barn owl, but is a useful concept in other species as well.

Chapter 5 Segregation of tectal and thalamic efferents in the barn owl's inferior colliculus

5.1 Introduction

Sound localization is mediated through neurons with spatially-limited receptive fields. This has been shown most convincingly in the barn owl, where these so-called space-specific neurons exist in multiple different areas in the brain. Two areas containing such neurons are particularly interesting: the optic tectum (OT; Knudsen 1983b) and the auditory portion of the archistriatum (AAr; Cohen and Knudsen 1995), for microstimulation in either of these nuclei leads to head saccades (du Lac and Knudsen 1990; Masino and Knudsen 1990; Knudsen *et al*. 1995). Moreover, lesion studies show that while either of these nuclei is sufficient for sound localization, at least one of them is necessary: pharmacological or electrolytic deactivation of one does not lead to a substantial loss of behavioral performance, but deactivation of both results in a total loss (Knudsen *et al*. 1993; Wagner 1993). This suggests that these nuclei mediate sound localization in parallel and are at least partially independent of one another. The goal of the present study is to determine to what extent the computations leading to the space-specific neurons in OT and AAr actually are independent of each other.

The barn owl computes the space-specificity observed in OT in three discrete steps. The principal sound localization cues, interaural time and intensity differences (ITD and IID, respectively), are computed separately in two brainstem nuclei from the sound pressure waveforms impinging on the two ears (step 1): nucleus laminaris (NL) contains neurons tuned to ITD (Moiseff and Konishi 1983; Carr and Konishi

1988), while nucleus ventralis lemnisci laterale, pars posterior (VLVp) is sensitive to IID (Moiseff and Konishi 1983; Manley *et al*. 1988; Takahashi and Keller 1992). NL and VLVp both project to the inferior colliculus (IC; Takahashi and Konishi 1988b; Takahashi and Keller 1992; Adolphs 1993b), creating neurons in the lateral shell subdivision (LS) sensitive to both ITD and IID (step 2; Feldman and Knudsen 1994; Mazer 1995; Keller and Takahashi 2000). LS neurons are still phase ambiguous, however, meaning that single neurons have multiple receptive fields across auditory space. It is not until a convergence of information across frequencies occurs (step 3; Takahashi and Konishi 1986) in the projection from LS to the external nucleus of the inferior colliculus (ICx) that phase ambiguity is resolved and space-specific neurons are formed. The space-specific properties of ICx neurons (Knudsen and Konishi 1978a) are essentially unchanged after they project to the deep layers of OT (Knudsen 1982; Knudsen and Knudsen 1983).

Some of the neural hardware leading to space-specificity in OT is shared with AAr. The pathway leading to AAr branches off from the OT pathway at the level of IC and goes through NO and field L before projecting to the archistriatum, of which AAr is the anterior 70% (Cohen *et al*. 1998). Hence, the computations performed in the brainstem (step 1) are used by both OT and AAr. It is less clear, however, whether the computations performed in IC (steps 2-3) are also shared. IC has been divided into four parts: the lateral (LS) and medial shells, and the core, all of which comprise the central nucleus (Takahashi and Konishi 1988b), plus the external nucleus (ICx; Knudsen and Konishi 1978a). While the boundary of IC as a whole is easily identified in a Nissl stain by ventricles and fiber tracts, the boundaries of the subdivisions within are more subtle and are defined by cell morphology (Knudsen 1983b), and acetylcholinesterase (Adolphs 1993a) and calcium-binding protein (Takahashi *et al*. 1987) stains. Nevertheless, it is generally believed that while LS projects to NO, ICx does not (Knudsen and Knudsen 1983; Proctor and Konishi 1997; Cohen *et al*. 1998), meaning that the computation of ITD-IID combination sensitivity (step 2) is shared, while the resolution of phase ambiguity (step 3) is not.

The present study addresses these issues through the use of a retrograde fluorescent double-labelling technique. Of particular interest is the apparent duplicity in the convergence of information across frequencies (step 3) occurring in both the midbrain and forebrain. To this end the projection patterns of neurons in LS and ICx were studied by simultaneously back-filling these cells with injections of different colored tracers into NO and OT. By illustrating the relative distribution of projection cells in IC and searching for the presence, or lack thereof, of any double-labelled cells, the data presented here further clarify which computations performed in IC are shared by the space-specific cells in OT and AAr.

5.2 Results

A total of 39 injections of fluorescent dextran amines were made in five optic tectums (OT) and six nucleus ovoidalises (NO) resulting in over 1700 retrogradely-labelled neurons in the inferior colliculus (IC) and other nearby nuclei (Tables 5.1 and 5.3). The exact locations of the injections were easily identifiable not only with fluorescent microscopy, but also with darkfield optics on the unstained sections due to small electrolytic lesions created by the injection protocol (Figs. 5.1 and 5.2). Scans for retrograde label were confined to transverse sections containing IC (Fig. 5.4) and focused largely on IC, the isthmal nuclei, and nearby auditory nuclei including the ventral nucleus of the lateral lemniscus (LLv) and the nuclei ventralis lemnisci laterale, pars posterior (VLVp) and pars anterior (VLVa).

Injection sites

The goal was to fill the target nucleus as much as possible. While most of NO was usually filled with four injections, OT was never completely filled even with six injections. This was due to the semi-circular canals limiting access to only the anterior half of OT when approached through the middle ear cavity. Nevertheless, excellent retrograde label from OT was seen not only in IC, but also in the isthmal nuclei, as

owl	OT inj.[1,2]	NO inj.[1,3]	OTp #[4]	NOp #[4]	dbl[5]	ovr[6]
659	1 F dp	1 R i	10	50	0	1
658	3 R int	4 F i+c	62	306	1	3
660	4 F int	6 R i	262	122	0	2
675	6 R int	4 F c	65	31	0	0
676	6 F dp+int	4 R i	386	64	0	5

Table 5.1: Summary of retrogradely-labelled cell counts. [1]F = fluorescein, R = rhodamine dextran amine. [2]dp = deep layers, int = intermediate layers of OT. [3]i = ipsilateral, c = contralateral to OT injection. [4]Number of neurons projecting to just optic tectum (OTp) or nucleus ovoidalis (NOp). [5]Double-labelled: number of neurons projecting to both optic tectum and nucleus ovoidalis. [6]Overlapped: number of OTp neurons amidst NOp neurons and vice versa.

quantified in Tables 5.1 and 5.3.

Of the 20 injections in OT, six were in the deep layers, 13 in the intermediate layers, and one on the boundary of the intermediate and deep layers. While dextran amine diffused into the superficial layers for some of the injections, the tectal ventricle prevented any from diffusing through the extracellular medium into IC. Figure 5.1 shows an example of three injection sites in OT. Clearly visible with darkfield microscopy (right) is the center of each injection site. Fluorescent microscopy (left) shows that the spread of dextran amine is limited to OT. This is typical of all of the injection sites in OT.

Of the 19 injections targeting NO, the centers, as well as the spread of dextran amine, of 18 were contained within its boundary. The one injection that was not a complete hit was in owl 676 on the border between NO, the occipitomesencephalic tract (OM), and tractus nucleus ovoidalis, the fiber tract leading from IC to NO. Coincidentally, this injection was also the smallest of all the injections. Figure 5.2 shows an example of two injection sites in NO. As with the injection sites in OT, the centers are clearly visible with darkfield microscopy. The spread of dextran amine is also limited to NO. With the one exception, this example is typical of the other injections.

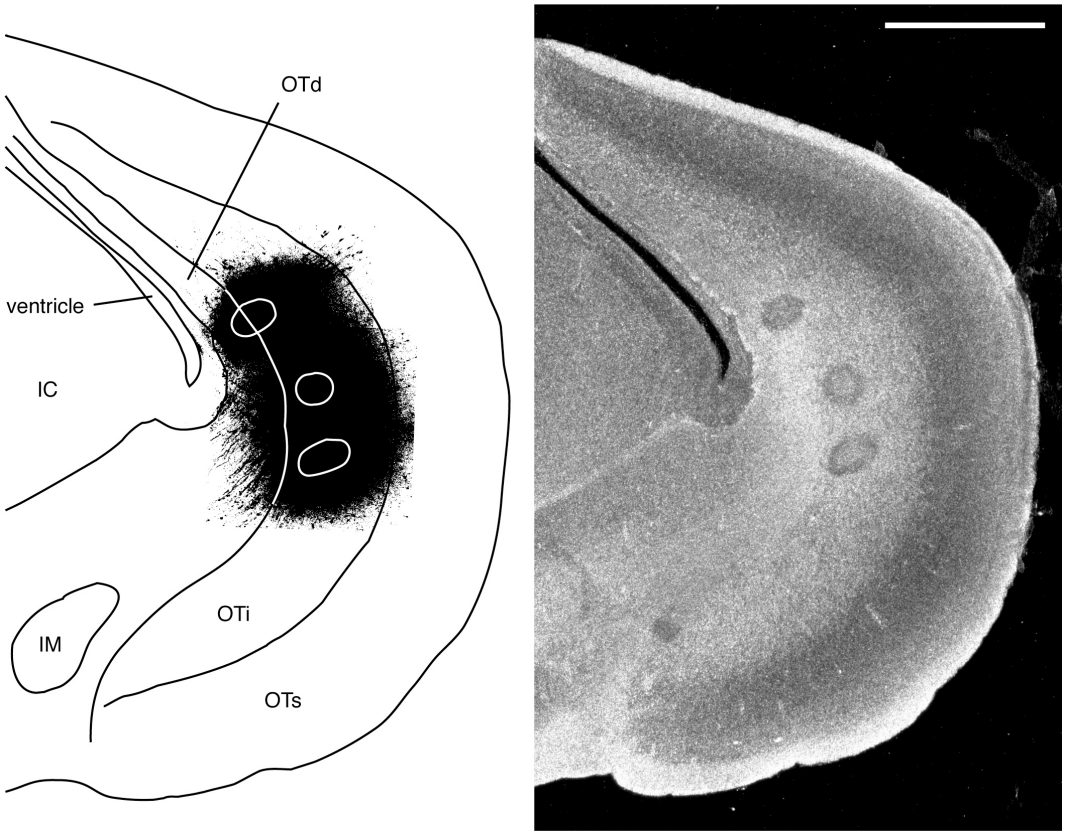

Figure 5.1: Injections of fluorescent retrograde label into the optic tectum (OT) of owl 676. On the right is a montage of three darkfield photomicrographs. Clearly visible are three lesions resulting from the injections. On the left is a montage of two confocal photomicrographs of the fluorescent label in the same section superimposed on a camera lucida drawing. This coronal section is 49% of the AP extent of OT from the anterior pole. Scale bar is 1000 μm; dorsal is up, medial is left. Inferior colliculus (IC); deep, intermediate, and superficial layers of the optic tectum (OTd, OTi, and OTs, respectively); magnocellular division of the isthmal nucleus (IM).

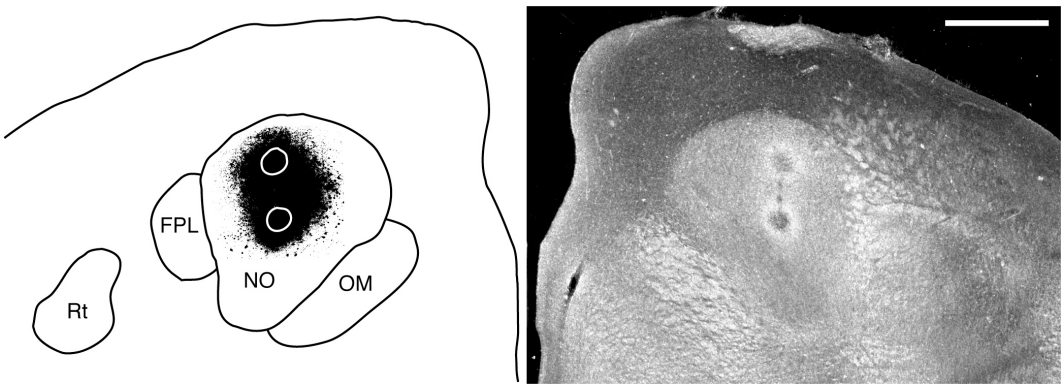

Figure 5.2: Injections of fluorescent retrograde label into nucleus ovoidalis (NO) of owl 676. On the right is a montage of four darkfield photomicrographs. Clearly visible are two lesions resulting from the injections, spaced about 700 μm apart in one dorsal-ventral penetration. On the left is a montage of two confocal photomicrographs of the fluorescent label in the same section superimposed on a camera lucida drawing. Orientation is flipped about the midline with respect to the photomicroph on the right. This coronal section is 43% of the AP extent of NO from the anterior pole. Scale bar is 1000 μm; dorsal is up. Rotundus (Rt); fasciculus proencephalic lateralis (FPL); occipitomesencephalic tract (OM).

Retrograde label

Scans for label transported outside of the injection sites were confined to retrograde label in and around IC. Figure 5.3 shows a montage of fluorescent photographs showing an example of the distribution of retrograde label from both OT and NO within IC. Neurons colored green project to OT, while red neurons project to NO. In this case, the OT-projecting neurons are in general clustered in the far lateral corner of IC, segregated from the NO-projecting neurons which are spread throughout the rest of IC. Figure 5.4 shows a camera lucida drawing of this section plus the rest of the sections containing IC in this owl. The image of Figure 5.3 corresponds to the middle left panel. As can be seen from the distribution of Xs and Os, the segregation of OT-projecting neurons from NO-projecting neurons, respectively, is consistent throughout all of IC. Moreover, this segregated distribution is present throughout all five owls in this study (data not shown).

Although the OT-projecting and NO-projecting neurons are in general segregated, a close examination of the distribution of these neurons reveals that there is some overlap in the two populations. Note, for example, the three neurons in Figure 5.3 which are not segregated: two NO-projecting (red) neurons on the medial side of and immediately adjacent to OT-projecting neurons, as well as one OT-projecting (green) neuron amidst the NO-projecting neurons. Figure 5.5 shows high-power magnifications of three more examples from owl 658. The left and middle panels show NO-projecting neurons completely surrounded by OT-projecting neurons. The right panel shows the only example in all five owls of a double-labelled neuron: one which projects to both OT and NO. In total, there are 12 such examples of overlapped or double-labelled neurons, accounting for 1.5% of the total number of OT-projecting neurons.

Neurons projecting to OT and NO have significantly different somal areas. Although the variance is quite large across owls, statistical comparisons within owls reveal that in four of the five owls, OT-projecting neurons are significantly larger

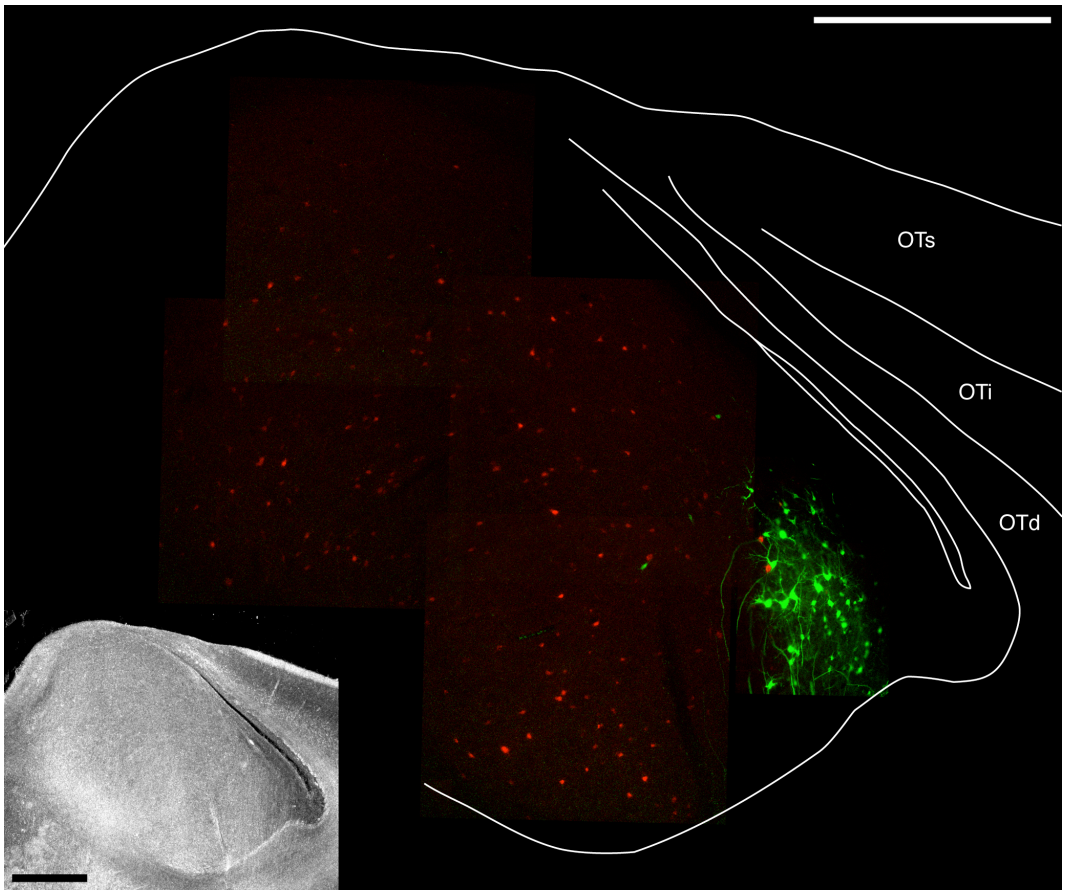

Figure 5.3: Fluorescent retrograde label in the inferior colliculus (IC) of owl 676, presented as a montage of six confocal photomicrographs superimposed on a camera lucida drawing. Neurons labelled green project to OT, while neurons labelled red project to NO. In general, OT-projecting neurons are segregated from NO-projecting neurons. But note the two NO-projecting neurons near the cluster of OT-projecting neurons, as well as the OT-projecting neuron in the cluster of NO-projecting neurons. Inset is a montage of four darkfield photomicrographs from the same section. This coronal section is 45% of the AP extent of IC from the anterior pole. Scale bar is 1000 μm in both cases; dorsal is up, medial is left. Abbreviations as in Figure 5.1.

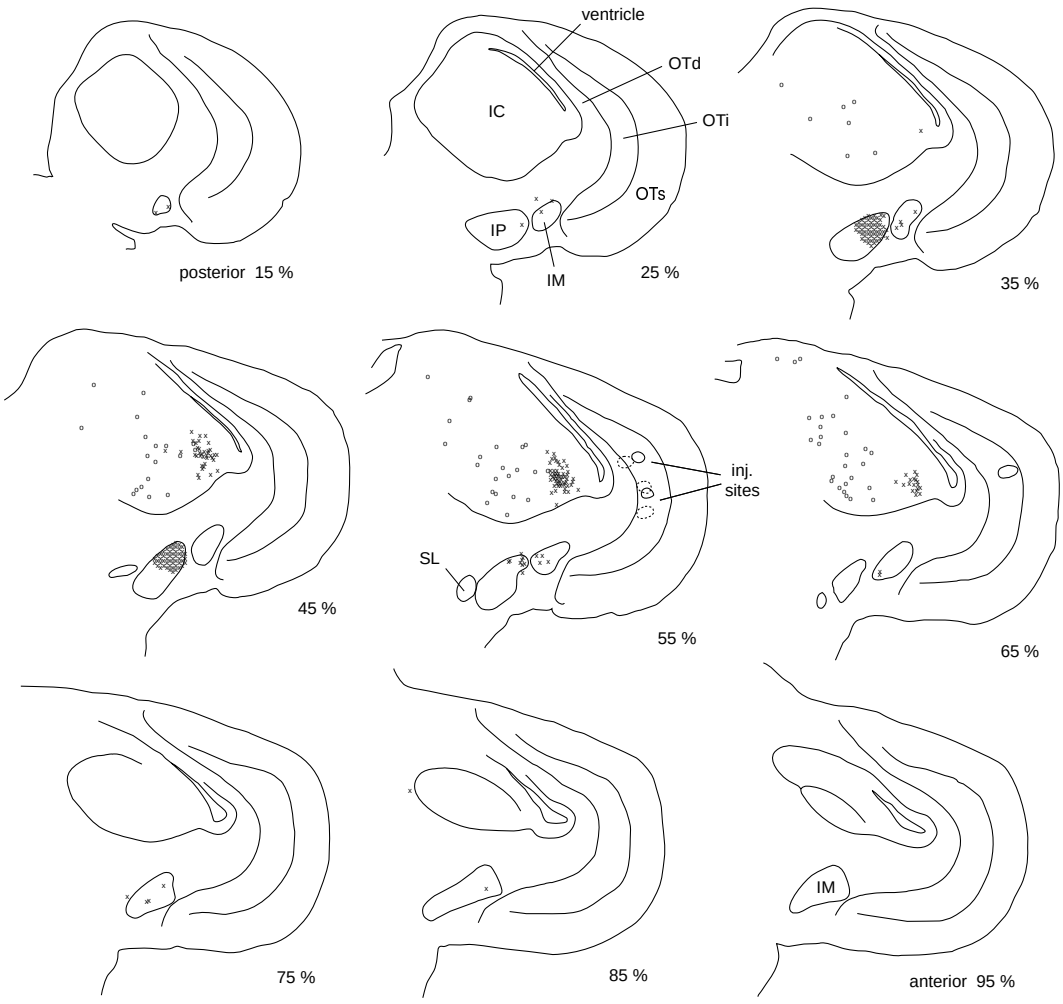

Figure 5.4: Nine camera-lucida drawn sections spanning the postero-anterior extent of IC in owl 676. Xs show neurons projecting to OT and Os show neurons projecting to NO. Drawings include retrogradely labelled neurons from intermediate sections in their approximate positions. Note the segregation between OT- and NO-projecting neurons, despite the small overlap in the sections labelled "45%" and "55%." The section of Figure 5.3 corresponds to the section labelled "45%" here. Coronal sections; dorsal is up, medial is left. Abbreviations as in Figure 5.1 plus parvocellular division of the isthmal nucleus (IP) and nucleus semilunaris (SL).

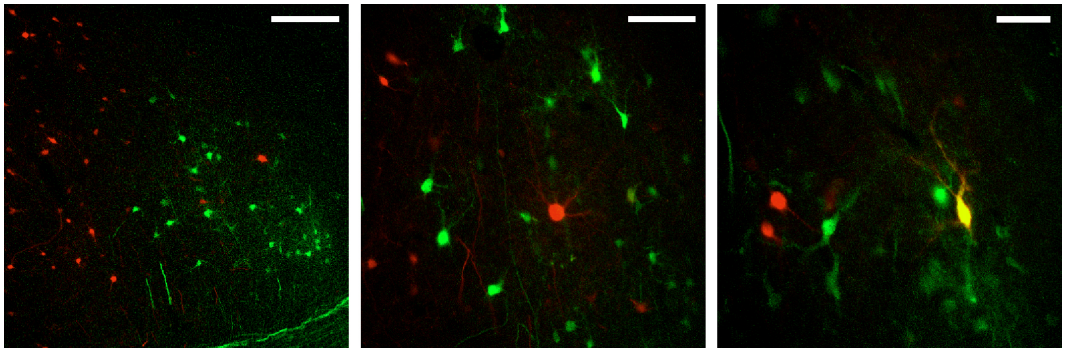

Figure 5.5: Two examples of the close proximity of neurons projecting to either OT or NO (left and center), plus the one exception of a neuron projecting to both OT and NO (right). Neurons labelled green project to OT, while neurons labelled red project to NO. Yellow indicates a projection to both nuclei. These coronal sections are 31, 38, and 27% of the AP extent of IC from the anterior pole, respectively, in owl 658. Scale bars are 250, 125, and 50 μm, respectively; dorsal is up, medial is left.

owl	OT inj.	NO inj.	OTp soma	NOp soma	p val
659	1 F dp	1 R i	236 ± 29	412 ± 20	< 0.0005
658	3 R int	4 F i+c	471 ± 17	420 ± 13	< 0.02
660	4 F int	6 R i	557 ± 21	385 ± 14	$< 10^{-8}$
675	6 R int	4 F c	432 ± 41	297 ± 30	< 0.02
676	6 F dp+int	4 R i	398 ± 22	341 ± 23	< 0.05

Table 5.2: Summary of retrogradely-labelled cell somal areas. Mean somal areas are in $\mu m^2 \pm$ SEM. n = 10, 60, 67, 19, and 44 for OTp and 50, 125, 58, 12, and 41 for NOp. Injection nomenclature is the same as in Table 5.1.

than NO-projecting neurons (Table 5.2). For the one owl in which this was not the case, NO-projecting neurons were of comparable size as such neurons in the other owls, while OT-projecting neurons were close to half the size seen in the other owls. The number of OT-projecting neurons labelled in this owl was the smallest across all birds and nuclei and it is possible that the inconsistency in the data is merely due to a sampling artifact.

Retrograde label was also found outside of IC. Neurons in contralateral nucleus semilunaris (SL) and the ipsilateral parvocellular (IP) and magnocellular (IM) divisions of the isthmal nucleus all project to OT (Table 5.3). By far, the most retrograde label among these three nuclei was found in ipsilateral IP: across five owls, there were over 300 retrogradely-labelled cell bodies. Interestingly, the label in IP was so dense that in some areas individual neurons could not be discerned unless the brightness and contrast settings of the microscope's photo-multiplier tubes were reduced. High-magnification observations revealed that the density of the fluorescence was due to the labelling of neural processes. As dextran amines travel both retrogradely and anterogradely (Glover *et al*. 1986; Vercelli *et al*. 2000) it was not possible to tell whether these processes were axons or dendrites. Figure 5.6 shows a particularly interesting section through the IP of owl 660 in which densely-labelled neural processes occurred in two stripes. Note the prominent dorso-medial to ventro-lateral stripe of fluorescence spanning the nucleus. A second stripe was visible between the two arrows when normal brightness and contrast settings were used, which were reduced in this image to reveal the underlying labelled cell bodies. While such dense labelling also occurred

owl	OT inj.	cSL	iIP	iIM
659	1 F dp	32	11+	2
658	3 R int	0	55	0
660	4 F int	0	90+	1
675	6 R int	1	51	1
676	6 F dp+int	3	104+	14

Table 5.3: Label outside of IC. Retrogradely-labelled neurons projecting to OT were observed in contralateral SL, ipsilateral IP, and ipsilateral IM. Plus (+) signs indicate the occurrence of densely-labelled neural processes. Injection nomenclature is the same as in Table 5.1.

in the IP of owls 659 and 676, only that of owl 659 occurred in a stripe: that of owl 676 encompassed the entire dorso-lateral half of the nucleus. This differential labelling pattern is likely a result of a single injection into OT in owl 659 versus multiple injections in owl 676.

Extremely sparse label was also observed bilaterally in LLv and contralaterally in VLVa after injections in NO. Such label was only observed in owl 676, however, and consisted of only two retrogradely-labelled neurons in ipsilateral LLv, two neurons in contralateral LLv, and three neurons in contralateral VLVa. Because owl 676 is the only owl in which one of the injections was not completely within the borders of NO, and because such label was not observed in any of the other four owls which received injections into NO, it seems likely that the label observed in LLv and VLVa represents fibers from the regions adjacent to NO.

Path of fiber tracts

The trajectory of fiber tracts between IC, NO, and OT was examined in two owls. Fibers projecting from IC to OT first extend ventrally into the medial efferent pathway, the prominent fiber tract just ventral to IC (Masino and Knudsen 1992; a.k.a. crossed-tectobulbar tract). Axons then course laterally underneath the tectal ventricle before diverging and entering OT. Such a trajectory was first described in the barn owl by Knudsen and Knudsen (1983).

Fibers projecting from IC to NO also start out by extending ventrally. But instead

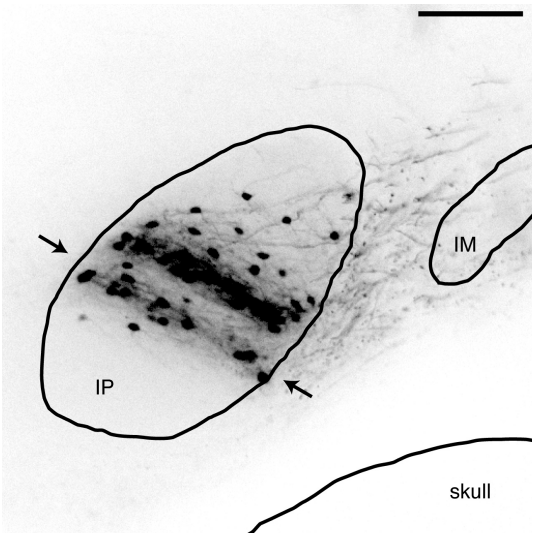

Figure 5.6: Fluorescent label in the parvocellular division of the isthmal nucleus (IP) of owl 660, presented as a confocal photomicrograph superimposed on a camera lucida drawing. In addition to the numerous retrogradely-labelled cell bodies, there was also a stripe of labelled neural processes extending from the dorso-medial edge to the ventro-lateral edge of the nucleus. This image was taken with reduced brightness and contrast settings for the photo-multiplier tubes of the microscope. When the normal setting were used, a second parallel stripe was visible between the two arrows and all of the labelled cell bodies within the two stripes were completely obscured. This coronal section is 50% of the AP extent of IP from the anterior pole. Scale bar is 500 μm; dorsal is up; medial is left. Magnocellular division of the isthmal nucleus (IM).

of changing course in the medial efferent pathway, they continue to course ventrally and pass between IP and IM before turning anteriorly near the skull. Bounded by IP medially, IM dorsally, OT laterally, and the skull ventrally they continue to course anteriorly until the level of the anterior most part of NO. They then turn dorsally and enter the tractus nucleus ovoidalis, which leads straight to NO (Proctor and Konishi 1997).

Extensive fiber label was also observed coursing medially in the medial efferent pathway after injections into OT. Such label crossed the midline and turned ventrally before becoming too dim to discern. Masino and Knudsen (1992) also observed such label after injections into OT and showed that it was anterograde label terminating in the motor nuclei controlling head saccades (see also Masino and Knudsen 1993 and Luksch *et al.* 2000). As dextran amines can be transported both retrogradely and anterogradely, however, the data presented here are consistent with a second intriguing possibility suggested by Figure 1 of both Peña and Konishi (2001) and Luksch *et al.* (2000): label is first retrogradely transported back to ICx and then anterogradely transported medially in the medial efferent pathway through a previously undescribed collateral branch of ICx axons with an unknown target zone.

5.3 Discussion

There are two pathways known to mediate sound localization in the barn owl. The midbrain pathway consists of space-mapped neurons in the optic tectum (OT; Knudsen 1983b), while the forebrain pathway consists of clusters of space-specific neurons in the auditory archistriatum (AAr; Cohen and Knudsen 1995). Interestingly, anatomical studies suggest that some of the computations leading to space-specificity may be duplicated: the branch point that the mid- and forebrain pathways have in common, the central nucleus of the inferior colliculus (ICc), does not contain space-specific neurons (Knudsen and Konishi 1978a; Cohen *et al.* 1998). This study, through a double-labelling technique more precise than those used in previous anatomical stud-

ies, reconfirms that cells in the inferior colliculus (IC) project either to OT or nucleus ovoidalis (NO), the first nucleus in the forebrain pathway, but not both. As it is commonly believed that only the space-mapped neurons in IC project to OT (Knudsen and Knudsen 1983), these results confirm that while the formation of ITD-IID combination sensitivity is likely shared between the two pathways, the resolution of phase ambiguity through frequency convergence is not.

The independence of the resolution of phase ambiguity in these two pathways is further supported by a spatial segregation within IC of neurons which project to OT and those which project to NO. While neurons projecting to OT were generally clustered in the lateral corner of IC, those projecting to NO were distributed throughout the rest of the nucleus. This segregation is not strict, however, as there is an intriguingly small percentage of retrogradely labelled neurons which lie amidst the cluster of neurons that project to the other nucleus. Though the number of such neurons is so small that they should rightly be considered outliers or exceptions, the striking juxtaposition of neurons with different projection targets makes one curious about the differences in physiology these neurons exhibit.

In addition to retrogradely-labelled cells in IC, there were also a large number of neurons retrogradely labelled in the parvocellular subdivision of the isthmal nucleus (IP). This projection from IP to OT has been previously documented not only in the barn owl (Knudsen and Knudsen 1983; Volman and Konishi 1989), but also in the pigeon (Hunt *et al.* 1977), and several mammalian species (rat: Watanabe and Kawana 1979; opossum: Méndez-Otero *et al.* 1980; cat: Roldán *et al.* 1983; monkey: Baizer *et al.* 1991; ferret: Jiang *et al.* 1996). While in birds the projection is ipsilateral only, in mammals it is bilateral. In all species, it terminates in the superficial layers of OT. Although the behavioral function of IP and its projection to OT are not known, Wang and colleagues have shown that IP neurons in the pigeon respond to visual stimuli, have receptive fields in the contralateral hemisphere, are arranged in a map, and inhibit the responses of OT neurons to visual stimuli (Wang and Frost 1991; Wang *et al.* 2000).

Bibliography

Abbas, P. J. and M. B. Sachs (1976). Two-tone suppression in auditory-nerve fibers: Extension of a stimulus-response relationship. *JASA 59*(1), 112–122.

Adolphs, R. (1993a). Acetylcholinesterase staining differentiates functionally distinct auditory pathways in the barn owl. *J. Comp. Neurol. 329*, 365–377.

Adolphs, R. (1993b). Bilateral inhibition generates neuronal responses tuned to interaural level differences in the auditory brainstem of the barn owl. *J. Neurosci. 13*(9), 3647–3668.

Albeck, Y. (1997). Inhibition sensitive to interaural time difference in the barn owl's inferior colliculus. *Hearing Res. 109*, 102–108.

Armstrong-James, M. and J. Millar (1979). Carbon fibre microelectrodes. *J. Neurosci. Meth. 1*, 279–287.

Baizer, J. S., J. F. Whitney, and D. B. Bender (1991). Bilateral projections from the parabigeminal nucleus to the superior colliculus in monkey. *Exp. Brain Res. 86*, 467–470.

Bala, A. D. S. and T. T. Takahashi (2000). Pupillary dilation response as an indicator of auditory discrimination in the barn owl. *J. Comp. Physiol. A 186*, 425–434.

Blauert, J. (1997). *Spatial Hearing: The Psycophysics of Human Sound Localization* (Revised ed.). MIT Press, Cambridge, Massachusetts.

Brainard, M. S., E. I. Knudsen, and S. D. Esterly (1992). Neural derivation of sound source location: Resolution of spatial ambiguities in binaural cues. *JASA 91*(2), 1015–1027.

Butler, R. A. (1986). The bandwidth effect on monaural and binaural localization. *Hearing Res. 21*(1), 67–73.

Carlile, S. (1990). The auditory periphery of the ferret. I: Directional response properties and the pattern of interaural level differences. *JASA 88*(5), 2180–2195.

Carr, C. E. and R. E. Boudreau (1991). Central projections of auditory nerve fibers in the barn owl. *J. Comp. Neurol. 314*, 306–318.

Carr, C. E., I. Fujita, and M. Konishi (1989). Distribution of GABAergic neurons and terminals in the auditory system of the barn owl. *J. Comp. Neurol. 286*, 190–207.

Carr, C. E. and M. Konishi (1988). Axonal delay lines for time measurement in the owl's brainstem. *PNAS 85*, 8311–8315.

Chandler, D. W. and D. W. Grantham (1992). Minimum audible movement angle in the horizontal plane as a function of stimulus frequency and bandwidth, source azimuth, and velocity. *JASA 91*(3), 1624–1636.

Chung, W., S. Carlile, and P. Leong (2000). A performance adequate computational model for auditory localization. *JASA 107*(1), 432–445.

Cohen, Y. E. and E. I. Knudsen (1995). Binaural tuning of auditory units in the forebrain archistriatal gaze fields of the barn owl: Local organization but no space map. *J. Neurosci. 15*(7), 5152–5168.

Cohen, Y. E., G. L. Miller, and E. I. Knudsen (1998). Forebrain pathway for auditory space processing in the barn owl. *J. Neurophys. 79*, 891–902.

Datum, M. S., F. Palmieri, and A. Moiseff (1996). An artificial neural network for sound localization using binaural cues. *JASA 100*(1), 372–383.

Delgutte, B. (1990). Two-tone rate suppression in auditory-nerve fibers: Dependence on suppressor frequency and level. *Hearing Res. 49*, 225–246.

Dowben, R. M. and J. E. Rose (1953). A metal-filled microelectrode. *Science 118*, 22–24.

du Lac, S. and E. I. Knudsen (1990). Neural maps of head movement vector and speed in the optic tectum of the barn owl. *J. Neurophys. 63*(1), 131–146.

Dyson, M. L., G. M. Klump, and B. Gauger (1998). Absolute hearing thresholds and critical masking ratios in the European barn owl: a comparison with other owls. *J. Comp. Physiol. A 182*, 695–702.

Egnor, R. (2000). *Cellular mechanisms for resolving phase ambiguity in the owl's inferior colliculus*. Ph. D. thesis, California Institute of Technology.

Ehret, G. and M. M. Merzenich (1985). Auditory midbrain responses parallel spectral integration phenomena. *Science 227*, 1245–1247.

Ehret, G. and M. M. Merzenich (1988). Complex sound analysis (frequency resolution, filtering and spectral integration) by single units of the inferior colliculus of the cat. *Brain Res. Rev. 13*, 139–163.

Ehret, G. and A. J. M. Moffat (1984). Noise masking of tone responses and critical ratios in single units of the mouse cochlear nerve and cochlear nucleus. *Hearing Res. 14*, 45–57.

Euston, D. R. and T. T. Takahashi (2002). From spectrum to space: The contribution of level difference cues to spatial receptive fields in the barn owl inferior colliculus. *J. Neurosci. 22*(1), 284–293.

Feldman, D. E. and E. I. Knudsen (1994). NMDA and non-NMDA glutamate receptors in auditory transmission in the barn owl inferior colliculus. *J. Neurosci. 14*(10), 5939–5958.

Fletcher, H. (1940). Auditory patterns. *Rev. Modern Phys. 12*, 47–65.

Fujita, I. and M. Konishi (1991). The role of GABAergic inhibition in processing of interaural time difference in the owl's auditory system. *J. Neurosci. 11*(3), 722–739.

Gill, D., L. Troyansky, and I. Nelken (2000). Auditory localization using direction-dependent spectral information. *Neurocomputing 32-33*, 767–773.

Gimlich, R. L. and J. Braun (1985). Improved fluorescent compounds for tracing cell lineage. *Dev. Biol. 109*, 509–514.

Glover, J. C., G. Petursdottir, and J. K. S. Jansen (1986). Fluorescent dextran-amines used as axonal tracers in the nervous-system of the chicken-embryo. *J. Neurosci. Meth. 18*(3), 243–254.

Gold, J. I. and E. I. Knudsen (2000). Abnormal auditory experience induces frequency-specific adjustments in unit tuning for binaural localization cues in the optic tectum of juvenile owls. *J. Neurosci. 20*(2), 862–877.

Hafter, E. R., R. H. Dye, J. M. Nuetzel, and H. Aronow (1977). Difference thresholds for interaural intensity. *JASA 61*(3), 829–834.

Hirsch, J. A., J. C. K. Chan, and T. C. T. Yin (1985). Responses of neurons in the cat's superior colliculus to acoustic stimuli. i. monaural and binaural response properties. *J. Neurophys. 53*(3), 726–745.

Hubel, D. H. (1957). Tungsten microelectrode for recording from single units. *Science 125*, 549–550.

Hunt, S. P., P. Streit, H. Künzle, and M. Cuénod (1977). Characterization of the pigeon isthmo-tectal pathway by selective uptake and retrograde movement of radioactive compounds and by golgi-like horseradish peroxidase labeling. *Brain Res. 129*, 197–212.

Irvine, D. R. F. and G. Gago (1990). Binaural interaction in high-frequency neurons in inferior colliculus of the cat: Effects of variations in sound pressure level on sensitivity to interaural intensity differences. *J. Neurophys. 63*(3), 570–591.

Jiang, Z. D., A. J. King, and D. R. Moore (1996). Topographic organization of projection from the parabigeminal nucleus to the superior colliculus in the ferret revealed with fluorescent latex microspheres. *Brain Res. 743*, 217–232.

Keller, C. H., K. Hartung, and T. T. Takahashi (1998). Head-related transfer functions of the barn owl: measurement and neural responses. *Hearing Res. 118*, 13–34.

Keller, C. H. and T. T. Takahashi (2000). Representation of temporal features of complex sounds by the discharge patterns of neurons in the owl's inferior colliculus. *J. Neurophys. 84*, 2638–2650.

King, A. J. and M. E. Hutchings (1987). Spatial response properties of acoustically responsive neurons in the superior colliculus of the ferret: A map of auditory space. *J. Neurophys. 57*(2), 596–624.

Knudsen, E. I. (1981). The hearing of the barn owl. *Sci. Amer. 245*, 113–125.

Knudsen, E. I. (1982). Auditory and visual maps of space in the optic tectum of the owl. *J. Neurosci. 2*(9), 1177–1194.

Knudsen, E. I. (1983a). Early auditory experience aligns the auditory map of space in the optic tectum of the barn owl. *Science 222*, 939–942.

Knudsen, E. I. (1983b). Subdivisions of the inferior colliculus in the barn owl (*Tyto alba*). *J. Comp. Neurol. 218*, 174–186.

Knudsen, E. I. (1984). Synthesis of a neural map of auditory space in the owl. In G. M. Edelman, W. M. Cowan, and W. E. Gall (Eds.), *Dynamic Aspects of Neocortical Function*, Chapter 11, pp. 375–396. John Wiley & Sons, New York.

Knudsen, E. I. and M. S. Brainard (1991). Visual instruction of the neural map of auditory space in the developing optic tectum. *Science 253*, 85–87.

Knudsen, E. I., Y. E. Cohen, and T. Masino (1995). Characterization of a forebrain gaze field in the archistriatum of the barn owl: Microstimulation and anatomical connections. *J. Neurosci. 15*(7), 5139–5151.

Knudsen, E. I. and P. F. Knudsen (1983). Space-mapped auditory projections from the inferior colliculus to the optic tectum in the barn owl (*Tyto alba*). *J. Comp. Neurol. 218*, 187–196.

Knudsen, E. I. and P. F. Knudsen (1985). Vision guides the adjustment of auditory localization in young barn owls. *Science 230*, 545–548.

Knudsen, E. I., P. F. Knudsen, and T. Masino (1993). Parallel pathways mediating both sound localization and gaze control in the forebrain and midbrain of the barn owl. *J. Neurosci. 13*(7), 2837–2852.

Knudsen, E. I. and M. Konishi (1978a). A neural map of auditory space in the owl. *Science 200*, 795–797.

Knudsen, E. I. and M. Konishi (1978b). Space and frequency are represented separately in auditory midbrain of the owl. *J. Neurophys. 41*(4), 870–884.

Knudsen, E. I. and M. Konishi (1979). Mechanisms of sound localization in the barn owl (*Tyto alba*). *J. Comp. Physiol. A 133*, 13–21.

Konishi, M. (1973). How the owl tracks its prey. *Amer. Sci. 61*, 414–424.

Konishi, M. (1986). Centrally synthesized maps of sensory space. *TINS 9*(4), 163–168.

Konishi, M. (1993). Neuroethology of sound localization in the owl. *J. Comp. Physiol. A 173*, 3–7.

Köppl, C. (1997). Phase locking to high frequencies in the auditory nerve and cochlear nucleus magnocellularis of the barn owl, *Tyto alba*. *J. Neurosci. 17*(9), 3312–3321.

Kuhn, G. F. (1977). Model for the interaural time differences in the azimuthal plane. *JASA 62*(1), 157–167.

Kuhn, G. F. (1979). The pressure transformation from a diffuse sound field to the external ear and to the body and head surface. *JASA 64*(4), 991–1000.

Kulkarni, A. and H. S. Colburn (1998). Role of spectral detail in sound-source localization. *Nature 396*, 747–749.

Lawrence, B. D. and J. A. Simmons (1982). Echolocation in bats: The external ear and perception of the vertical positions of targets. *Science 218*, 481–483.

Lu, Z. and R. R. Fay (1996). Two-tone interaction in primary afferents and midbrain neurons of the goldfish, *Carassius Auratus*. *Auditory Neurosci. 2*, 257–273.

Luksch, H., B. Gauger, and H. Wagner (2000). A candidate pathway for a visual instructional signal to the barn owl's auditory system. *J. Neurosci. 20*(RC70), 1–4.

Manley, G. A., C. Köppl, and M. Konishi (1988). A neural map of interaural intensity differences in the brain stem of the barn owl. *J. Neurosci. 8*(8), 2665–2676.

Marrese, C. A. (1987). Preparation of strongly adherent platinum black coatings. *Analytical Chem. 59*(1), 217–218.

Masino, T. and E. I. Knudsen (1990). Horizontal and vertical components of head movement are controlled by distinct neural circuits in the barn owl. *Nature 345*(6274), 434–437.

Masino, T. and E. I. Knudsen (1992). Anatomical pathways from the optic tectum to the spinal cord subserving orienting movements in the barn owl. *Exp. Brain Res. 92*, 194–208.

Masino, T. and E. I. Knudsen (1993). Orienting head movements resulting from electrical microstimulation of the brainstem tegmentum in the barn owl. *J. Neurosci. 13*(1), 351–370.

Mazer, J. A. (1995). *Integration of Parallel Processing Streams in the Inferior Colliculus of the Barn Owl*. Ph. D. thesis, California Institute of Technology.

Mazer, J. A. (1998). How the owl resolves auditory coding ambiguity. *PNAS 95*, 10932–10937.

Mendelson, J. R. and K. L. Grasse (2000). Auditory cortical responses to the interactive effects of interaural intensity disparities and frequency. *Cerebral Cor-*

tex 10(1), 32–39.

Méndez-Otero, R., C. E. Rocha-Miranda, and V. H. Perry (1980). The organization of the parabigemino-tectal projections in the opossum. *Brain Res. 198*, 183–189.

Middlebrooks, J. C. and D. M. Green (1991). Sound localization by human listeners. *Annu. Rev. Psychol. 42*, 135–159.

Middlebrooks, J. C. and E. I. Knudsen (1984). A neural code for auditory space in the cat's superior colliculus. *J. Neurosci. 4*(10), 2621–2634.

Mills, A. W. (1960). Lateralization of high-frequency tones. *JASA 32*(1), 132–134.

Moiseff, A. (1989a). Bi-coordinate sound localization by the barn owl. *J. Comp. Physiol. A 164*, 637–644.

Moiseff, A. (1989b). Binaural disparity cues available to the barn owl for sound localization. *J. Comp. Physiol. A 164*, 629–636.

Moiseff, A. and M. Konishi (1981). Neuronal and behavioral sensitivity to binaural time differences in the owl. *J. Neurosci. 1*(1), 40–48.

Moiseff, A. and M. Konishi (1983). Binaural characteristics of units in the owl's brainstem auditory pathway: Precursors of restricted spatial receptive fields. *J. Neurosci. 3*(12), 2553–2562.

Moore, B. C. J., D. A. Vickers, C. J. Plack, and A. J. Oxenham (1999). Inter-relationship between different psychoacoustic measures assumed to be related to the cochlear active mechanism. *JASA 106*(5), 2761–2778.

Mori, K. (1997). Across-frequency nonlinear inhibition by GABA in processing of interaural time difference. *Hearing Res. 111*, 22–30.

Musicant, A. D., J. C. K. Chan, and J. E. Hind (1990). Direction-dependent spectral properties of cat external ear: New data and cross-species comparisons. *JASA 87*(2), 757–781.

Nandy, D. and J. Ben-Arie (2001). Neural models for auditory localization based on spectral cues. *Neurological Res. 23*, 489–500.

Nelken, I., P. J. Kim, and E. D. Young (1997). Linear and nonlinear spectral integration in type IV neurons of the dorsal cochlear nucleus. II. predicting responses with the use of nonlinear models. *J. Neurophys. 78*, 800–811.

Neti, C., E. D. Young, and M. H. Schneider (1992). Neural network models of sound localization based on directional filtering by the pinna. *JASA 92*(6), 3140–3156.

Norberg, R. A. (1977). Occurrence and independent evolution of bilateral ear asymmetry in owls and implications on owl taxonomy. *Phil. Trans. Roy. Soc. Lond. B 280*, 375–408.

Olsen, J. F., E. I. Knudsen, and S. D. Esterly (1989). Neural maps of interaural time and intensity differences in the optic tectum of the barn owl. *J. Neurosci. 9*(7), 2591–2605.

Palmer, A. R. and A. J. King (1982). The representation of auditory space in the mammalian superior colliculus. *Nature 299*, 248–249.

Payne, R. S. (1971). Acoustic location of prey by barn owls (*Tyto alba*). *J. Exp. Biol. 54*, 535–573.

Peña, J. L. and M. Konishi (2000). Cellular mechanisms for resolving phase ambiguity in the owl's inferior colliculus. *PNAS 97*(22), 11787–11792.

Peña, J. L. and M. Konishi (2001). Auditory spatial receptive fields created by multiplication. *Science 292*, 249–252.

Peña, J. L., S. Viete, Y. Albeck, and M. Konishi (1996). Tolerance to sound intensity of binaural coincidence detection in the nucleus laminaris of the owl. *J. Neurosci. 16*(21), 7046–7054.

Pittman, Jr., C. U., W. Jiang, Z. R. Yue, and C. A. Leon y Leon (1999). Surface area and pore size distribution of microporous carbon fibers prepared by electrochemical oxidation. *Carbon 37*, 85–96.

Poganiatz, I. and H. Wagner (2001). Sound-localization experiments with barn owls in virtual space: influence of broadband interaural level difference on head-turning behavior. *J. Comp. Physiol. A 187*, 225–233.

Proctor, L. and M. Konishi (1997). Representation of sound localization cues in the auditory thalamus of the barn owl. *PNAS 94*, 10421–10425.

Rayleigh, Lord (1876). Our perception of the direction of a source of sound. *Nature 14*, 32–33.

Rayleigh, Lord (1906). On our perception of sound direction. *Phil. Mag. J. Science 13*, 214–232.

Roldán, M., F. Reinoso-Suárez, and A. Tortelly (1983). Parabigeminal projections to the superior colliculus in the cat. *Brain Res. 280*, 1–13.

Rosenzweig, M. R. (1961). Development of research on the physiological mechanisms of auditory localization. *Psych. Bull. 58*(5), 376–389.

Rumelhart, D., G. Hinton, and R. Williams (1986). Learning internal representations by error propagation. In D. Rumelhart and J. McClelland (Eds.), *Parallel Distributed Processing: Explorations in the Microstructure of Cognition Vol 1: Foundations*. MIT Press, Cambridge.

Saberi, K., H. Farahbod, and M. Konishi (1998). How do owls localize interaurally phase-ambiguous signals? *PNAS 95*, 6465–6468.

Saberi, K., Y. Takahashi, H. Farahbod, and M. Konishi (1999). Neural bases of an auditory illusion and its elimination in owls. *Nature Neuro. 2*(7), 656–659.

Sachs, M. B. and N. Y. S. Kiang (1968). Two-tone inhibition in auditory-nerve fibers. *JASA 43*(5), 1120–1128.

Schreiner, C. E. and G. Langner (1997). Laminar fine structure of frequency organization in auditory midbrain. *Nature 388*, 383–386.

Sullivan, W. E. and M. Konishi (1984). Segregation of stimulus phase and intensity coding in the cochlear nucleus of the barn owl. *J. Neurosci. 4*(7), 1787–1799.

Takahashi, T. and M. Konishi (1986). Selectivity for interaural time difference in the owl's midbrain. *J. Neurosci. 6*(12), 3413–3422.

Takahashi, T., A. Moiseff, and M. Konishi (1984). Time and intensity cues are processed independently in the auditory system of the owl. *J. Neurosci. 4*(7), 1781–1786.

Takahashi, T. T., C. E. Carr, N. Brecha, and M. Konishi (1987). Calcium binding protein-like immunoreactivity labels the terminal field of nucleus laminaris of the barn owl. *J. Neurosci. 7*(6), 1843–1856.

Takahashi, T. T. and C. H. Keller (1992). Commissural connections mediate inhibition for the computation of interaural level difference in the barn owl. *J. Comp. Physiol. A 170*, 161–169.

Takahashi, T. T. and M. Konishi (1988a). Projections of nucleus angularis and nucleus laminaris to the lateral lemniscal nuclear complex of the barn owl. *J. Comp. Neurol. 274*, 212–238.

Takahashi, T. T. and M. Konishi (1988b). Projections of the cochlear nuclei and nucleus laminaris to the inferior colliculus of the barn owl. *J. Comp. Neurol. 274*, 190–211.

Takahashi, T. T., H. Wagner, and M. Konishi (1989). Role of commissural projections in the representation of bilateral auditory space in the barn owl's inferior colliculus. *J. Comp. Neurol. 281*, 545–554.

Venturi, J. B. (1796). Considerations sur la connaissance de l'tendue que nous donne le sens de l'ouie. *Magasin encyclopedique, ou journal des sciences, des lettres et des arts 3*(9), 29–37. (in Landmarks of Science II)

Vercelli, A., M. Repici, D. Garbossa, and A. Grimaldi (2000). Recent techniques for tracing pathways in the central nervous system of developing and adult mammals. *Brain Res. Bull. 51*(1), 11–28.

Volman, S. F. and M. Konishi (1989). Spatial selectivity and binaural responses in the inferior colliculus of the great horned owl. *J. Neurosci. 9*(9), 3083–3096.

Wagner, H. (1993). Sound-localization deficits induced by lesions in the barn owl's auditory space map. *J. Neurosci. 13*(1), 371–386.

Wang, Y., j. Xiao, and S.-R. Wang (2000). Excitatory and inhibitory receptive fields of tectal cells are differentially modified by magnocellular and parvocellular divisions of the pigeon nucleus isthmi. *J. Comp. Physiol. A 186*, 505–511.

Wang, Y.-C. and B. J. Frost (1991). Visual response characteristics of neurons in the nucleus isthmi magnocellularis and nucleus isthmi parvocellularis of pigeons. *Exp. Brain Res. 87*, 624–633.

Watanabe, K. and E. Kawana (1979). Efferent projections of the parabigeminal nucleus in rats: a horseradish peroxidase (HRP) study. *Brain Res. 168*, 1–11.

Wise, L. Z. and D. R. F. Irvine (1985). Topographic organization of interaural intensity difference sensitivity in deep layers of cat superior colliculus: Implications for auditory spatial representation. *J. Neurophys. 54*(2), 185–211.

Wong, D. (1984). Spatial tuning of auditory neurons in the superior colliculus of the echolocating bat, *Myotis lucifugus. Hearing Res. 16*, 261–270.

Wotton, J. M., T. Haresign, and J. A. Simmons (1995). Spatially dependent acoustic cues generated by the external ear of the big brown bat, *Eptesicus fuscus. JASA 98*(3), 1423–1445.

Yost, W. A. and R. H. Dye, Jr. (1988). Discrimination of interaural differences of levels as a function of frequency. *JASA 83*(5), 1846–1851.